Lithos 396–397 (2021) 106195

Contents lists available at ScienceDirect

Lithos

journal homepage: www.elsevier.com/locate/lithos

Research Article

Systematic LREE enrichment of mantle harzburgites: The petrogenesis of San Carlos xenoliths revisited

Romain Tilhac [a,b,*], Tomoaki Morishita [a], Natsumi Hanaue [a], Akihiro Tamura [a], Juan Miguel Guotana [a]

[a] Faculty of Geosciences and Civil Engineering, Kanazawa University, Kanazawa 920-1192, Japan
[b] Instituto Andaluz de Ciencias de la Tierra (IACT), CSIC – Universidad de Granada, 18100 Armilla, Granada, Spain

ARTICLE INFO

Article history:
Received 3 March 2021
Received in revised form 26 April 2021
Accepted 26 April 2021
Available online 30 April 2021

Keywords:
Flux melting
Open-system melting model
Reactive channeling instability
Pressure-solution creep
Tectonic reactivation
Jemez Lineament

ABSTRACT

The dichotomy between partial melting and metasomatism is a paradigm of mantle geochemistry since the pioneering work of Frey and Prinz (1978) on the occurrence of LREE-enriched harzburgites. However, the thermo-chemical implications of such two-stage scenarios are often poorly considered, and the latter fail to explain why trace-element enrichment and major-element depletion are often proportional. We here re-envisage the petrogenesis of the famous San Carlos peridotites based on new petrographic observations and detailed modal, major- and trace-element compositions. The lherzolites (and pyroxenites) are characterized by homogeneously fertile mineral chemistry and LREE-depleted patterns consistent with low degrees of partial melting of the lherzolitic protolith. Bulk compositions and mineral zoning suggest that opx-rich pyroxenites formed by pressure-solution creep during melt-present deformation, locally accompanied by magmatic segregations of cpx. The harzburgites are characterized by stronger mineral zoning with low-Mg# and Na-, Al- and Cr-rich cpx rims, and can be discriminated in a low-Jd and high-Jd cpx groups. The high-Jd group is interpreted as the result of local elemental redistribution in the presence of a low-degree hydrous melt, in good agreement with their wide range of LREE enrichment. In contrast, the MREE-to-HREE fractionation and increasing Cr# in spinel of the low-Jd group indicate that they experienced higher degrees of melting. Open-system melting simulations of trace-element fractionation during hydrous flux melting suggests that the high-Jd harzburgites are the result of low fluid influx producing poorly extracted melt, while higher influx led to higher melting degrees and efficient melt extraction in the low-Jd harzburgites; the lherzolites mostly remained below or near solidus during that process. The lithological and chemical heterogeneity of San Carlos mantle is thus compatible with a single-stage evolution, which is also supported by the striking consistency between Fe-Mg exchange and REE thermometric estimates (1057 and 1074 °C on average, respectively), indicating that harzburgites and lherzolites probably followed a similar P-T path and relatively little sub-solidus re-equilibration. These interpretations suggest that the development of melt extraction pathways promoted by reactive channeling instability is able to produce complex lithological heterogeneities during hydrous flux melting. This process provides a self-consistent explanation for the systematic enrichment of harzburgites observed in many mantle terranes and xenoliths worldwide. We argue that San Carlos is one of such examples where a *ca* 1.5-Ga continental lithosphere experienced localized flux melting and deformation during the tectonic reactivation of a Proterozoic subduction zone, providing new constraints on the mantle sources of volcanic activity in the Jemez Lineament.

1. Introduction

The paradoxical association of light rare earth element (LREE)-depleted fertile lherzolites and LREE-enriched harzburgites has long been controversial in mantle petrology. While lherzolites are compatible with variable degrees of partial melting and/or refertilization (*e.g.* Le Roux et al., 2007), the major and trace-element compositions (*i.e.* characteristic U-shaped or spoon-shaped REE patterns) of harzburgites have been variously ascribed to crustal contamination (Gruau et al., 1998), melt metasomatism (Song and Frey, 1989) or the presence of melt inclusions (Garrido et al., 2000). Although certainly valid in specific cases, these two-staged scenarios fail to explain why LREE enrichment is almost systematically proportional to major-element depletion, as evidenced by correlations between $(La/Sm)_N$ and melt extraction indexes such as MgO or Yb (Frey and Prinz, 1978). Additional mechanisms are required to make refractory peridotites more susceptible and/or exposed to subsequent re-enrichment or to the entrapment of LREE-enriched melt. It had been envisaged that the lithospheric mantle was

* Corresponding author at: Instituto Andaluz de Ciencias de la Tierra (IACT), CSIC – Universidad de Granada, 18100 Armilla, Granada, Spain.
E-mail address: romain.tilhac@csic.es (R. Tilhac).

https://doi.org/10.1016/j.lithos.2021.106195

zoned in such a way that harzburgites lie deeper and are more exposed to upcoming metasomatic fluids and melts (Frey and Prinz, 1978), but this is not consistent with the compositional stratification observed in different tectonic contexts (Griffin et al., 2003). The greater melt connectivity (and permeability) of olivine-rich assemblages is also often invoked (Toramaru and Fujii, 1986), but the validity of this approach inferring melt distribution and geometry from dihedral angle is limited to low melt fractions and large grain sizes (Garapić et al., 2013 and references therein). Furthermore, higher olivine modes are not systematically observed in the most LREE-enriched harzburgites. Alternatively, percolation-reaction models have been used to ascribed LREE/MREE enrichment and HREE depletion to chromatographic re-equilibration accompanying partial melting and melt migration (Vernières et al., 1997). This view is supported by nearly identical LREE concentrations in coexisting orogenic lherzolites and harzburgites (*e.g.* Downes, 2001). However, in spite of their elegance, such single-stage scenarios that, in fact, combine melt extraction and percolation remain somewhat coincidental. Furthermore, chromatography is conditioned by fast diffusional re-equilibration between melt and minerals. While early formulations assumed solid diffusivities of 10^{-12} cm^2/s (Vasseur et al., 1991), more recent experimental estimates of REE diffusivities in clinopyroxene (cpx) are many orders of magnitude slower, in the range of 10^{-18} to 10^{-21} cm/s (Van Orman et al., 2001). It is likely that not only lithospheric melt percolation but also partial melting occurs in disequilibrium (Oliveira et al., 2020; Tilhac et al., 2020, and references therein), such as envisaged early on by Prinzhofer and Allègre (1985).

A strong constraint on the origin of mantle peridotites is provided by field observations (see Bodinier and Godard, 2014 for a review). The occurrence of refractory peridotites as small and irregular bodies or layers among fertile peridotites in exposed terranes is strongly incompatible with various extents of melting degrees resulting from pressure and/or temperature variations which require unrealistic thermal gradients (Kelemen et al., 1992). A line of reasoning accounting for this observation consists in considering layering as a product of multiple deformation episodes (Toramaru et al., 2001). Melt-peridotite interaction associated with melt percolation through, and from, dykes and high-porosity channels are also invoked (*e.g.* Bodinier et al., 2004; Dygert et al., 2016), and the compositional consequences of these processes are often referred to as *metasomatism*. While this term originally referred to mineralogical changes (encompassing metamorphic reactions) before being restricted to the *"enrichment of the rock by new substances"* (Goldschmidt, 1922), we note that it is mainly used in the mantle literature to refer to "*the introduction and/or removal of chemical components*" while *"the rock remains in a solid state"* (Harlov and Austrheim, 2013) – in other words, any open-system sub-solidus process. It is a convenient geochemical definition, but somewhat ambiguous because it has unclear, yet implicit thermo-chemical implications. For instance, melt-induced metasomatism requires melt sources and P-T conditions that allow for the percolating melt to coexist with the percolated protolith. Similarly, in the absence of petrographic evidence for modal metasomatism, partial melting or breakdown reactions, fluid-induced metasomatism must be limited to a narrow range of P-T conditions below the wet peridotite solidus and above the stability field of hydrous/volatile-bearing phases (phlogopite, mica, amphibole, *etc.*). These considerations reflect the limitations of a reasoning based on discrete magmatic processes and specifically the dichotomy between magmatism and metasomatism (see also Kiseeva et al., 2017) and an ongoing paradigm change. Recent studies indeed increasingly emphasize on the importance of characterizing the origin and distribution of mantle heterogeneities (Katz and Weatherley, 2012; Sanfilippo et al., 2019), and notably pyroxene-rich lithologies (Lambart et al., 2013), water and other volatiles (*e.g.* Keller and Katz, 2016).

To contribute to this paradigm change, we re-envisage the petrogenesis of San Carlos xenolith suite, Arizona (USA), whose origin and evolution are mostly limited to the pioneering work of Frey and Prinz (1978). Based on new detailed observations and major- and trace-element compositions, we argue that (1) the lithological and chemical diversity of San Carlos harzburgites, lherzolites and pyroxenites can be mostly explained by a single-stage flux melting episode, owing to the inherent spatial variability of this complex process; and that (2) the paradoxical occurrence of LREE-depleted fertile lherzolites and LREE-enriched harzburgites may often reflect the development of melt extraction pathways controlled by pre-existing heterogeneities and the presence of volatiles.

2. Geology and petrography of San Carlos xenoliths

San Carlos is a small (<50 km^2), Miocene to Quaternary volcanic field located in the San Carlos Apache Indian Reservation. The samples studied are from the Peridot Mesa, a vent/flow complex comprising a diatreme (Peridotite Hill) and alkaline-rich basanite flow (Hadnott et al., 2017; Wohletz, 1978) dated at 0.58 ± 0.21 Ma by K-Ar ages (Bernatowicz, 1981). Mantle xenoliths occur as bombs or loose rocks, and as gravity-settled masses particularly abundant in Peridot Canyon where they represent >50% of the flow volume (Frey and Prinz, 1978). The locality is famous for providing high concentrations of fresh, coarse-grained (gem-quality) olivine widely used as a geoscience standard.

Based on their classification of basalt inclusions, Frey and Prinz (1978) discriminated San Carlos xenoliths into the volumetrically dominant Group I (Cr-diopside lherzolite) and subordinate Group II (Al-augite wehrlite-pyroxenite). Compared to the Mg-, Cr-rich (Group-II) spinel peridotites and pyroxenites, Group-II xenoliths are Fe- and Ti-richer, mineralogically more diverse and somehow cogenetic to the host basanites, as supported by their nearly identical Sr-isotope compositions. However, their petrogenesis remain ambiguous in the absence of unequivocal cumulate textures and they are not included in this study.

We have selected a representative set of samples for detailed investigation, which covers most of the petrological and mineralogical diversity of San Carlos Group-I xenoliths (Fig. 1): 4 harzburgites, 2 lherzolites and a composite lherzolite-pyroxenite sample (SH01). They have well equilibrated xenomorphic granular textures (*e.g.* Fig. 1a), varying from coarse mosaic equigranular (400 μm to 1 mm) to porphyroclastic (200 μm to 2 mm). The latter is particularly observed in cpx-rich areas where grain size is reduced (Fig. 1d), while cpx-free areas are coarser-grained (2 to 5 mm; Fig. 1b). These textural variations define layers or patches, commonly observed in San Carlos lherzolites where modal compositions are locally pyroxenitic, with variable orthopyroxene (opx) proportions. This is the case in sample SH01 whose bulk composition is comparable to other lherzolite samples but also exhibits a lherzolitic (SH01-R) and an olivine-websteritic part (SH01-L), the latter further subdivided into near-parallel, opx-rich and opx-poor bands (Fig. 1e, see also Fig. 5). In harzburgites and low-opx lherzolites, opx is commonly found enclosed in olivine and cpx form interstitial opx-free aggregates, locally with large amoeboid spinel (300 μm to 2 mm) enclosing cpx and/or olivine grains. In lherzolites and the opx-rich parts of harzburgites, cpx, opx and spinel are associated and olivine inclusions are found in opx and/or cpx. In these samples, cpx and spinel are preferentially located in contact with both olivine and opx, particularly where these assemblages are necked between olivine grains. Composite textures where cpx-spinel and opx-cpx-spinel assemblages coexist are also found, mostly in harzburgites (*e.g.* Fig. 1c). Poikilitic textures with large (>5 mm) opx enclosing blocky xenomorphic olivine grains are locally observed (Fig. 1f).

Grain boundaries are curvilinear and triple junctions are dominant between silicates. Olivine is fresh and exhibit sub-grain boundaries and kink bands in large grains. Clinopyroxene is mostly unstrained but may exhibit spongy rims (see Fig. 7d & e) and low dihedral angle when in contact to other minerals, olivine in particular. Orthopyroxene is blocky, locally fractured and rare fine cpx exsolution are found in large grains. Spinel is internally homogeneous and mostly occurs interstitially

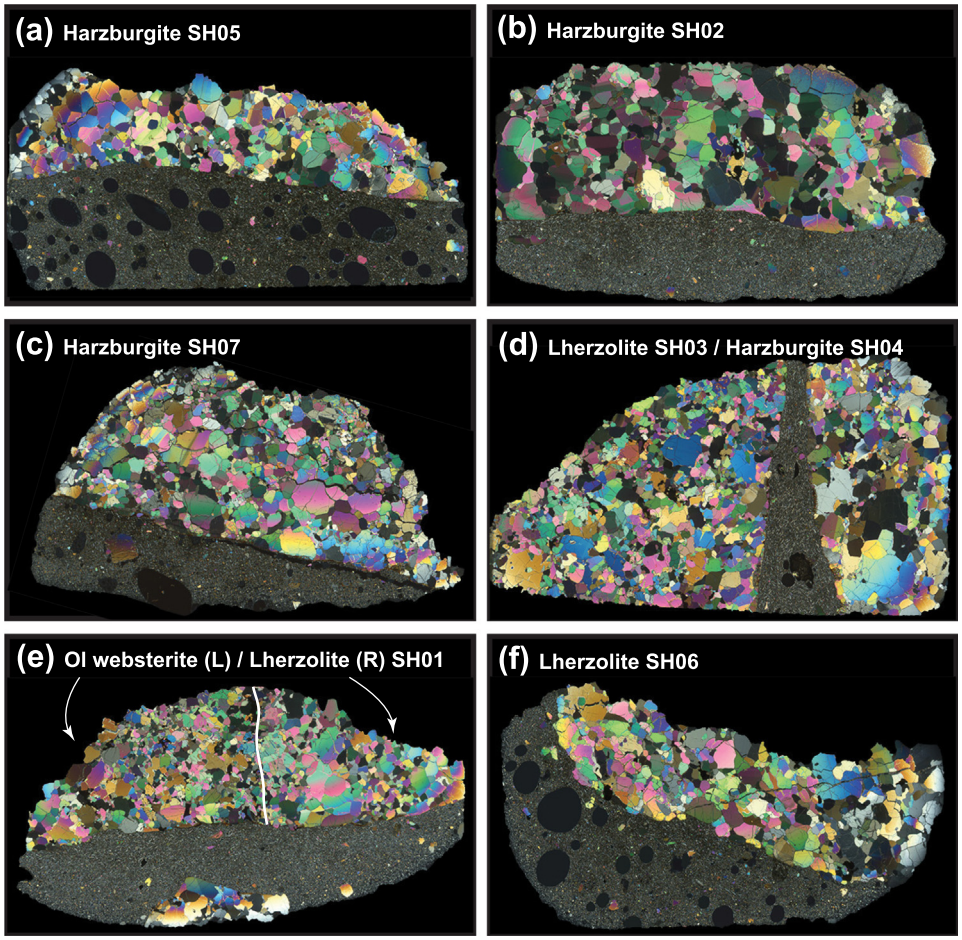

Fig. 1. Photomicrographs (cross-polarized light) of thin sections of xenoliths analyzed in this study: high-Jd (a & c) and low-Jd (b & d) harzburgites, and lherzolites (d, e and f). See text and Fig. 5 for more detail on heterogeneous sample SH01.

with rare exceptions being curbed inclusions in silicates (Frey and Prinz, 1978); it is rarely associated with phlogopite and/or pargasitic amphibole in harzburgites. Veins variously containing glass, plagioclase microlites and spinel have been described by Frey and Prinz (1978).

3. Modal, major- and trace-element compositions

All data and analytical methods are reported in Electronic Appendix 1.

3.1. Modal compositions and mineral chemistry

Modal compositions of San Carlos peridotite xenoliths are reported in Table 1 and shown in Fig. 2. Overall, the modal abundance of cpx, opx and spinel decrease with increasing abundance of olivine and this correlation is particularly well defined for opx (Electronic Appendix 2a). Clinopyroxene/opx ratios also roughly decrease with increasing abundance of olivine, spanning from relatively low in harzburgites (0.07–0.12; one sample reaches 0.35) to a relatively wide range in lherzolites (0.21–1.1).

Mineral chemistry is consistent to a first order with these modal variations (Fig. 3 and Electronic Appendix 2b). Forsterite (Fo) content in olivine increases with the modal abundance of olivine (Electronic Appendix 2a), but olivine has relatively lower Fo in samples with high cpx/opx. In both pyroxenes, Al_2O_3 decreases linearly with increasing Mg# and this trend is particularly steep in harzburgites (Fig. 3a and Electronic Appendix 2b). TiO_2 also roughly decreases with increasing Mg#, but lherzolites and harzburgites differ markedly in being TiO_2-rich and TiO_2-poor, respectively (Fig. 3c). Clinopyroxene and opx exhibit homogeneous Na_2O in lherzolites while the latter steeply decreases with increasing Mg# in harzburgites (Fig. 3d), defining a

Table 1
Mineralogy and thermometry of San Carlos peridotites and pyroxenites.

wt%	Olivine	Opx	Cpx	Spinel	T_{BKN} (°C)	T_{REE} (°C)
Harzburgites						
SH02	79.2	18.5	1.3	1.0	1043	1049 ± 25
SH04	65.5	31.1	2.6	0.8	1090	1179 ± 28
SH05	70.1	25.6	3.0	1.2	1062	1007 ± 28
SH07	81.3	13.4	4.5	0.8	1029	1018 ± 27
Lherzolites						
SH01-R	70.7	14.0	15.1	0.2	1017	1066 ± 58
SH03	55.7	26.5	15.6	2.2	1088	1071 ± 31
SH06	48.4	40.4	8.0	3.2	1110	1111 ± 53
Pyroxenites						
SH01-L*	18.7	52.3	24.5	4.5	1017	1057 ± 26

Surface proportions were obtained from X-ray elemental maps and converted to weight percentages using mineral densities calculated from end-member mineral proportions following Tilhac et al. (2016). * SH01-L corresponds the pyroxenitic part of heterogeneous sample SH01 (see text for further detail). T_{BKN} and T_{REE} are temperature estimates from the two-pyroxene (Brey and Köhler, 1990) and REE-in-two-pyroxene thermometer (Liang et al., 2013), respectively, both calculated using average core compositions. The reported REE temperatures were obtained excluding the lightest REE (La-Nd), although robust regression yields nearly identical results (see Electronic Appendix 3) as all REE are mostly in near equilibrium between the pyroxenes.

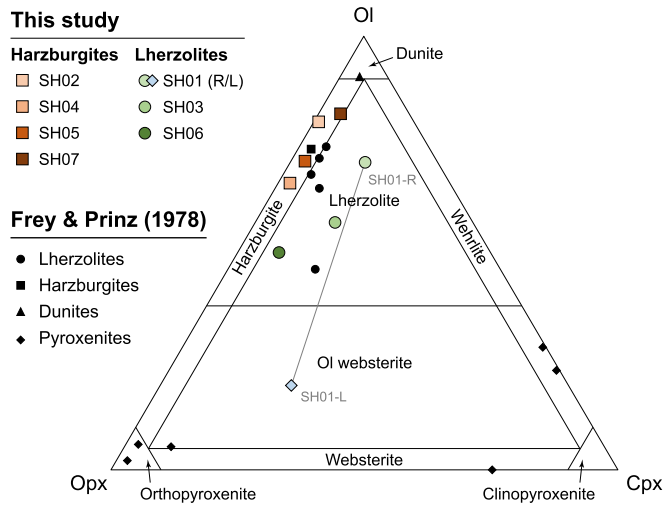

Fig. 2. Modal compositions of San Carlos peridotites from this study and Frey and Prinz (1978) recalculated into olivine (ol), clinopyroxene (cpx) and orthopyroxene (opx) proportions (Table 1). The line connects the two parts (pyroxenitic and lherzolitic) of heterogeneous sample SH01 (see Fig. 5).

high-Na_2O and low-Na_2O groups thereafter referred to as high-jadeite (Jd) and low-Jd groups. Cr_2O_3 increases with increasing Mg# in both pyroxenes, except the low-Jd group which exhibit relatively low Cr_2O_3 at a given Mg# compared to other harzburgites (Fig. 3b). Petrographically, the low-Jd group of harzburgites is characterized by the textural association of cpx and opx and the abundance of olivine inclusions in opx, while cpx is more commonly observed as single-phase interstitial assemblage within olivine in the high-Jd group. In good agreement with mineral chemistry in pyroxenes, Cr# in spinel increases nearly linearly with increasing Fo content in olivine (Fig. 4). In particular, harzburgitic spinels are discriminated in a high-Cr# and a low-Cr# groups coinciding with the high-Jd and low-Jd cpx groups, respectively. In contrast, all lherzolitic spinel plot together except in sample SH03, which has the lowest Cr# among the studied xenoliths.

In addition to the variability described above between and within lherzolites and harzburgites, several samples exhibit significant variations at the cm-scale, as previously noted by Wilshire and Jackson (1975). To reflect this variability, we selected a composite sample (SH01; Fig. 5a) where Mg# in cpx increases at the contact between a lherzolitic and an olivine-websteritic layer (Fig. 5b). This evolution is accompanied by a marked increase in Al_2O_3 (and to a lesser extent Cr_2O_3) and a slight decrease in TiO_2 across the olivine-websteritic part. These trends in Al_2O_3 and TiO_2 are also observed in opx while the Fo content of olivine varies to a lesser extent. No consistent variation in the mineral

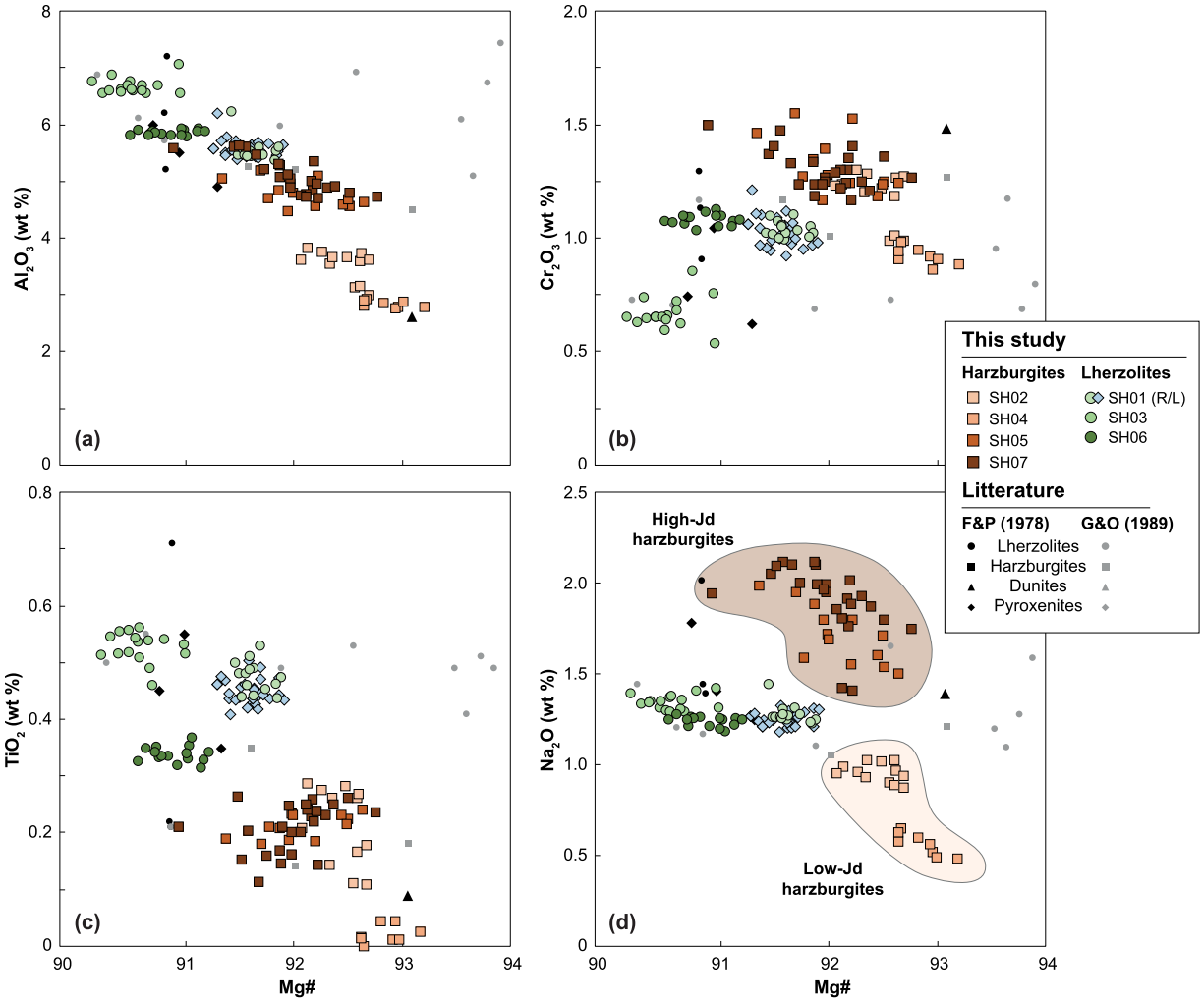

Fig. 3. Mineral chemistry of cpx: Al_2O_3 (a), Cr_2O_3 (b), TiO_2 (c) and Na_2O (d) *vs* Mg# [molar 100 ×Mg / (Mg + total Fe^{2+})]. *High-Jd* and *low-Jd harzburgites* respectively refer to harzburgitic cpx with high and low jadeite (Jd) contents (see text for more detail). Compositions from Frey and Prinz (1978) and Galer and O'Nions (1989) are shown for comparison.

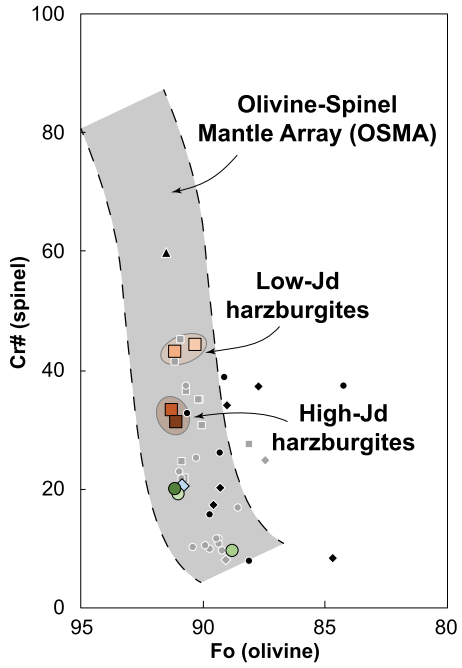

Fig. 4. Cr# [molar 100 × Cr / (Cr + Al)] of spinel *vs* Fo content (%) of olivine compared to the Olivine-Spinel Mantle Array (OSMA) of Arai (1994). Symbols as in Fig. 3.

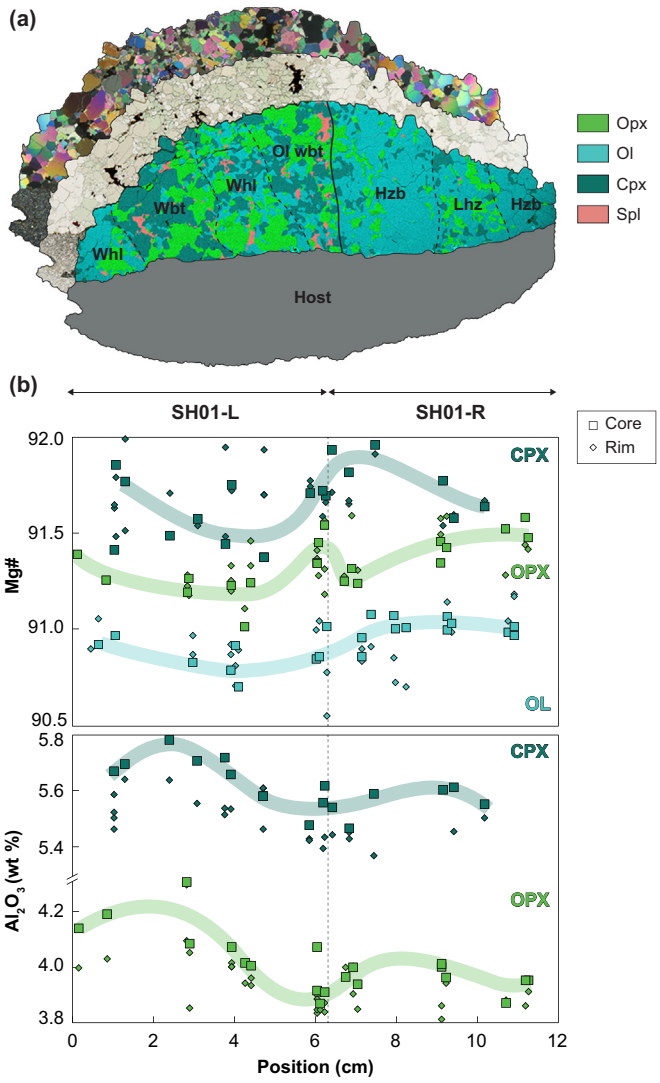

Fig. 5. Elemental (X-ray) map showing the evolution of modal compositions in heterogeneous sample SH01 (a), and corresponding compositional profiles of Mg# and Al_2O_3 in cpx and opx across the sample (b).

chemistry of olivine, cpx, opx or spinel are observed towards the contact with the host basanite indicating the absence of contamination from the lava.

At the mineral scale, slight but significant variations in major-element compositions have also been observed (Fig. 6), particularly in harzburgites (Fig. 7). Clinopyroxene cores have higher Mg# and this zoning is stronger in harzburgites, and especially the low-Mg# samples (*i.e.* high-Jd group). In lherzolites, cpx core are slightly richer in Al_2O_3 (up to ~0.6 wt%), and to a lesser extent Cr_2O_3 (with slightly lower Mg#) than the rims, particularly in cpx-rich domains such as the olivine-websteritic part of sample SH01. In harzburgites, the opposite situation is observed (with few exceptions) and cpx cores exhibit lower Al_2O_3 (by up to ~0.9 wt%), Cr_2O_3 and Na_2O (Fig. 7), and to a lesser TiO_2 (with slightly higher Mg#) than the rims. The strongest differences in Na_2O are observed in the high-Jd group of harzburgites where cpx rims are up ~0.5 wt% richer than the cores (Figs. 6 & 7d-e). Detailed profiles across selected harzburgitic cpx grains show that these variations in cpx are little sensitive to the nature of neighboring minerals or the textural assemblage and that no plateau composition are preserved at the core (Fig. 7). With few exceptions, core-to-rims variations in opx and olivine are less significant and systematic, and no differences have been observed between harzburgites and lherzolites or between textural assemblages.

3.2. Trace-element compositions

San Carlos harzburgites and lherzolites are markedly different in their trace-element compositions. In lherzolites, cpx have LREE-depleted patterns (Fig. 8a) with $(La/Sm)_N = 0.27–0.41$ positively correlated to the Yb concentration and are homogeneous at sample and mineral scale. These patterns contrast with the wide range of MREE-to-HREE slopes [$(Gd/Yb)_N = 0.5–2.9$] and LREE enrichment observed in harzburgites where $(La/Sm)_N = 1.1–1.6$ is roughly negatively correlated to the Yb concentration. The lowest HREE concentrations are found in the low-Jd harzburgites which also exhibit the widest variability of MREE-to-HREE slopes. On the other hand, high-Jd harzburgites have a wider range of LREE enrichment and exhibit variations both at the sample and mineral scale. For instance, LREE-enriched cpx rims coexist with spoon-shaped to LREE-enriched rims. Extended trace-element spider diagrams show markedly negative high field strength element (HFSE) anomalies (Fig. 8b) with Zr-Hf fractionation ranging from homogeneously low $(Zr/Hf)_N$ in lherzolites to higher values in harzburgites, and particularly the low-Jd group (Fig. 9). Lherzolitic cpx are also characterized by slightly negative Sr anomalies [$(Sr/Sr^*)_N = 0.7–0.8$] and low concentrations of fluid-mobile elements such as Th and U. These observations contrast with variously enriched Th and U in harzburgites and weakly (low-Jd group) to strongly (high-Jd group) positive Sr anomalies [$(Sr/Sr^*)_N = 1.0–2.9$]. No significant changes have been observed in the trace-element compositions of cpx with respect to the distance to the host basanite.

Orthopyroxenes exhibit uniformly depleted REE patterns in both harzburgites and lherzolites with homogeneous MREE-to-HREE slopes (Fig. 8c). As for cpx, harzburgitic opx have lower bulk HREE contents and are less LREE-depleted than their lherzolitic counterparts. Similarly, Sr anomalies tend to be negative in lherzolites and positive in harzburgites (Fig. 8d). Zr-Hf fractionation is comparable to that observed in cpx, with a marked difference between harzburgites with low $(Zr/Hf)_N$ and lherzolites with higher values. With few exceptions,

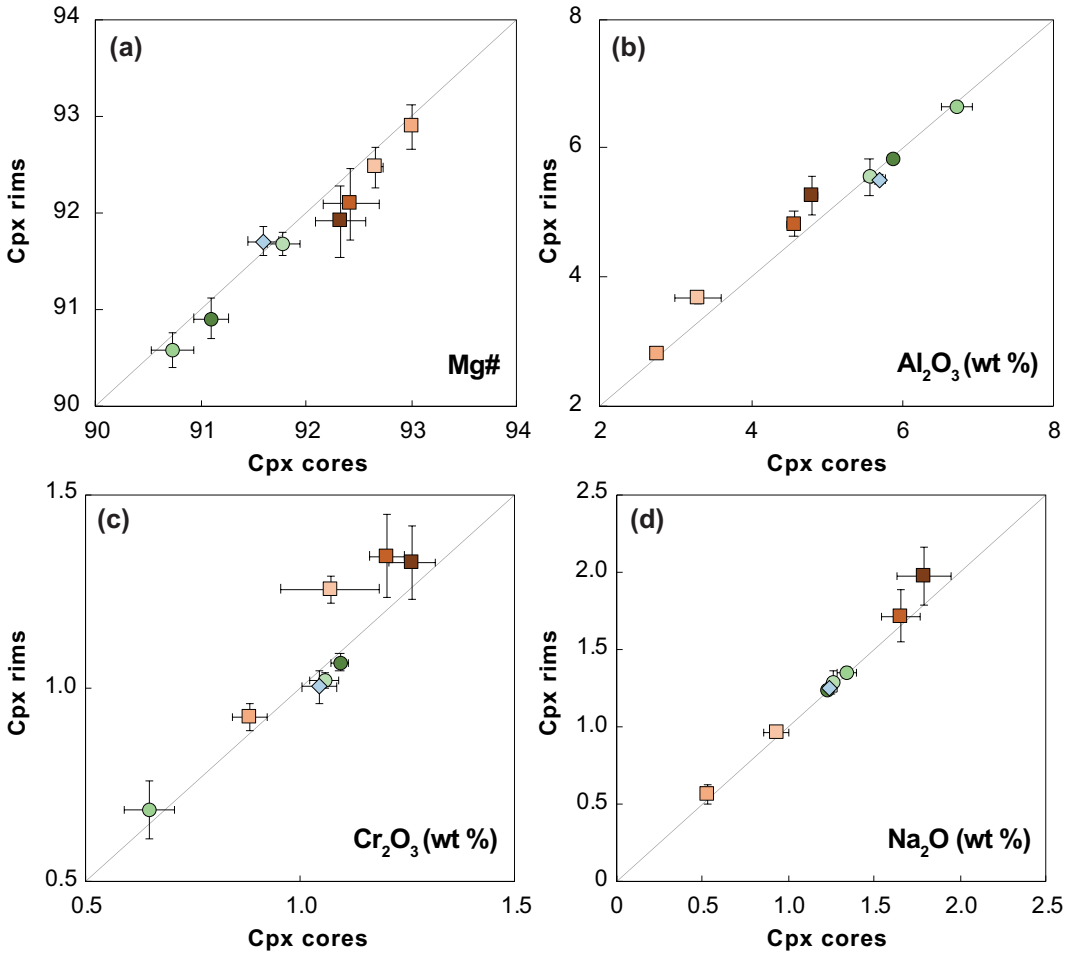

Fig. 6. Average core-to-rim variations of Mg# (a), Al_2O_3 (b), Cr_2O_3 (c) and Na_2O (d) in cpx. Error bars indicate the standard deviation (1σ) for each sample. Note the lower Mg# and higher Al_2O_3 and Cr_2O_3 concentrations (and higher Na_2O for the high-Jd group) in the rims of harzburgitic cpx.

the trace-element compositions of opx are homogeneous within error at both sample and mineral scale.

4. Discussion

4.1. Lherzolite fertility and the origin of pyroxenites

Negative correlation between the concentration of basaltic components and the MgO content of peridotites is commonly interpreted as reflecting varying degrees of melt extraction (*e.g.* Bodinier and Godard, 2014). In San Carlos xenoliths, there is a 3 wt% drop in Al_2O_3 over ~10 wt% MgO between the most fertile lherzolites and most refractory harzburgites. Depending on the melting model and conditions considered (Herzberg, 2004), around 20% melt extraction are required to account for such compositional evolution (Fig. 10a), which is consistent with the associated decrease in HREE concentrations. For instance, the observed decrease in the Yb content of cpx from 1.70 to 0.25 ppm can be accounted for by a degree (F) of non-modal batch melting of 22% (or 14% if fractional) using a dry lherzolite melting reaction of a Depleted MORB Mantle (DMM) source. It is consistent with the Cr# measured in spinel corresponding to F ~ 15–18% using the empirical formulation of Hellebrand et al. (2001). This interpretation is also consistent with the limited increase in the concentration of compatible elements such as Ni, Co and Sc, as pointed out by Frey and Prinz (1978). They indeed reported ~30% increase in whole-rock Ni concentrations coherent with our bulk-rock reconstructions (*e.g.* 11–37% increase in NiO between lherzolites and harzburgites). Such a moderate increase is comparable to the 25% increase expected from the range of F considered above, assuming a bulk partition coefficient ~10, while fractional crystallization would have much stronger effect over similar melt fractions.

To a first order, San Carlos lherzolites and harzburgites can be considered as residues of relatively low and high degrees of melting, respectively. As suggested for other lherzolites worldwide, fertility may also relate to a refertilization process (*e.g.* Le Roux et al., 2007) rather than solely to low-degrees of partial melting. Their bulk compositions exceed, notably in terms of SiO_2 (~46 wt%), DMM (SiO_2 = 44.7 wt%; Workman and Hart, 2005) and even Primitive Upper Mantle (PUM) estimates (44.9 wt%; McDonough and Sun, 1995) (Fig. 10a). The lherzolites are also intermediate between harzburgites and pyroxenites in such a way that a process equivalent to mixing harzburgitic residues with a "pyroxenitic" component could be envisaged. The lherzolites indeed have lower FeO and higher SiO_2 than expected from lower melting degrees (with respect to the harzburgites), which trend towards the pyroxenite compositions (Figs. 10b and 11c). However, the recent overprint of San Carlos harzburgites inferred from their relatively homogeneous Nd-isotope compositions certainly excludes that the latter represent the pre-refertilization protolith (Galer and O'Nions, 1989). In other words, if the apparent fertility of San Carlos lherzolites is potentially the result of a refertilization process, their protolith and the actual process are poorly recorded. Nonetheless, the lherzolitic and pyroxenitic cpx (Fig. 3d), and to a lesser extent opx, exhibit strikingly

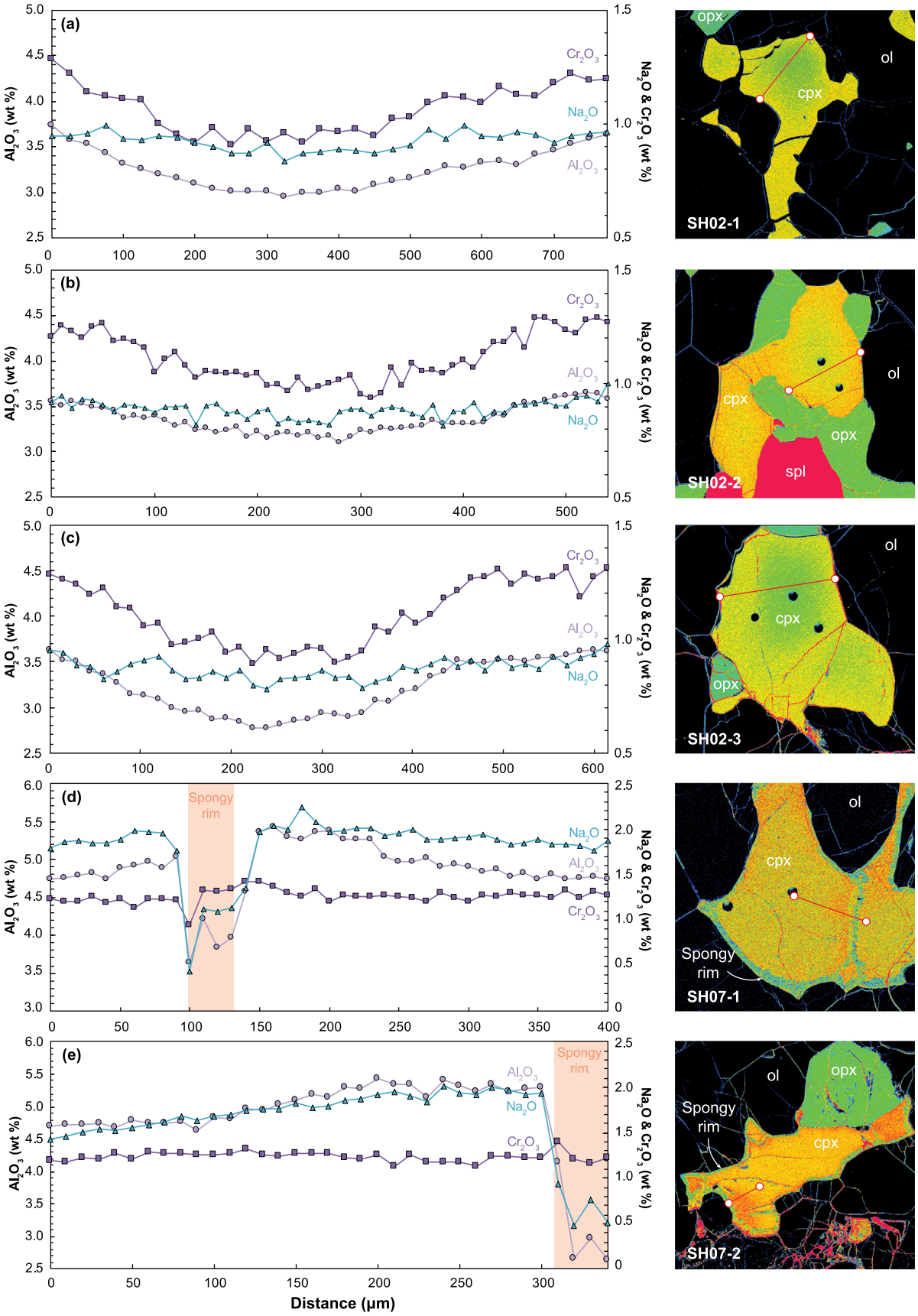

Fig. 7. Detailed core-to-rim (or rim-to-rim) profiles of Al_2O_3 (left Y axis) and Cr_2O_3 and Na_2O (right Y axis) concentrations in the low-Jd (a-c) and high-Jd (d-e) harzburgitic cpx. The profile locations are indicated by the red line on the X-ray map of Al_2O_3 concentrations. Note the symmetrical increase in Al_2O_3 and Cr_2O_3 towards the rims in SH02 regardless of the neighboring mineral and the marked increase in Al_2O_3 and Na_2O in SH07. Pits left after LA-ICP-MS analysis are visible in some cpx.

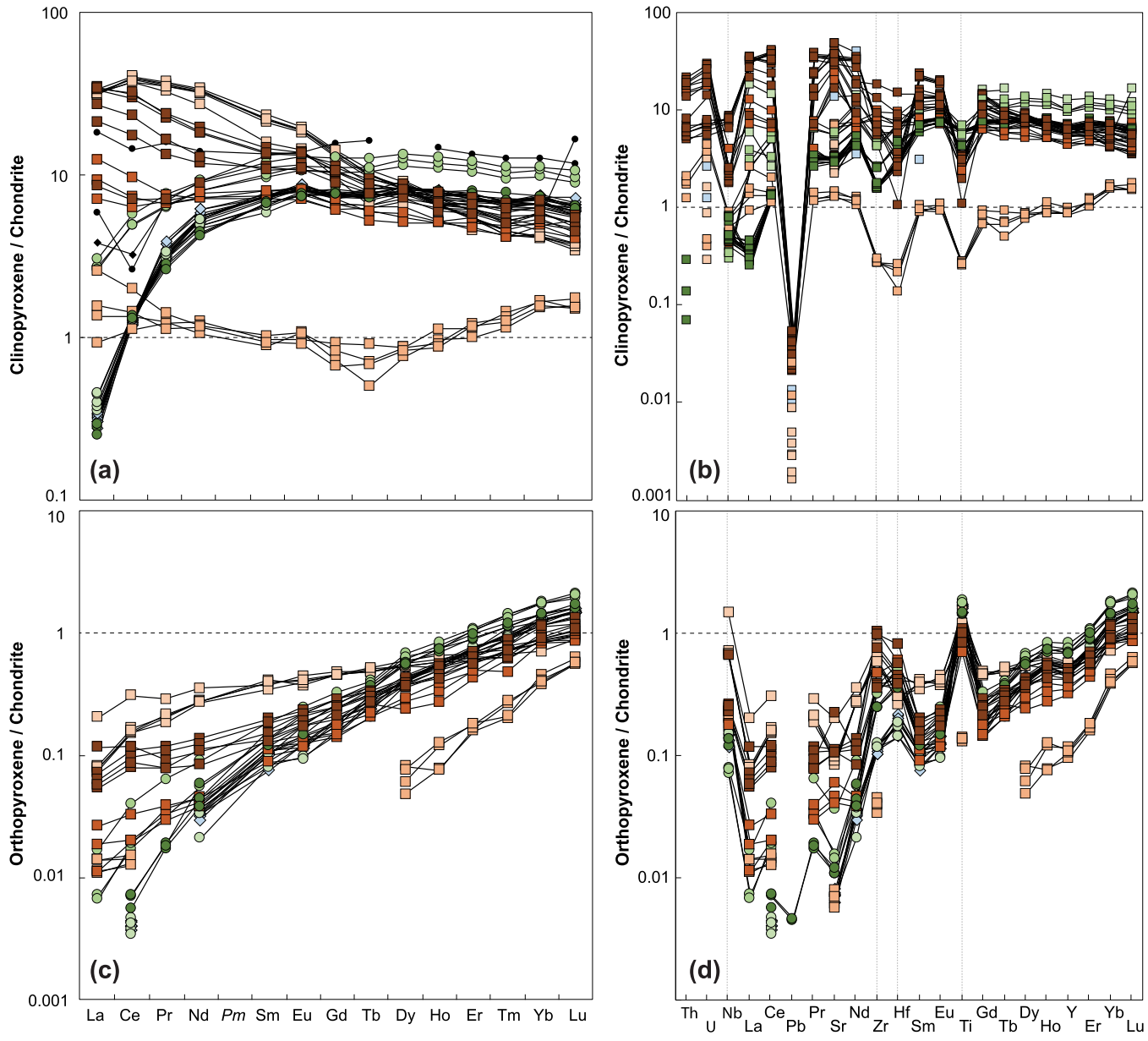

Fig. 8. Chondrite-normalized REE (a & c) and multi-element spider (b & d) diagrams for cpx (a & b) and opx (c & d). Symbols as in Fig. 3. Chondrite composition after McDonough and Sun (1995).

homogeneous Na_2O (1.2–1.4 wt%) and similarly LREE-depleted patterns, suggesting that the pyroxenites and lherzolites formation are certainly not unrelated.

4.1.1. Metamorphic segregation of pyroxenes

Two main models classically account for pyroxenite formation in the upper mantle (see Downes, 2007 for a review): the recycling of oceanic crust and the crystallization of percolating melts variously reacting with the host peridotites. While the former is often invoked but poorly documented (*e.g.* Chetouani et al., 2016 and references therein), the latter has been widely discussed (Borghini et al., 2020; Garrido and Bodinier, 1999; Gysi et al., 2011; Tilhac et al., 2016) and a variety of potential melt sources have been identified (Lu et al., 2018; Lu et al., 2020). In contrast, earlier models of *"in-situ"* pyroxenite formation *via* partial melting or pyroxene segregation during deformation (Dick and Sinton, 1979) have remained unpopular and perhaps overlooked in the absence of experimental and theoretical data.

We argue that metamorphic segregations of pyroxenes may explain the formation of opx-rich pyroxenitic layers in San Carlos lherzolites (and elsewhere) and the close similarities between their mineral compositions. To test this hypothesis, we postulate that the bulk pyroxenite compositions resulting from such a process should approximate a mixing line between the compositions of the lherzolitic pyroxenes. This is indeed observed in most oxides as illustrated for Na_2O (*vs* MgO) in Fig. 11a but the pyroxenites also exhibit a negative correlation between Mg# and Cr# that cannot be solely explained by mixing lherzolitic cpx and opx components. The latter exhibit a positive correlation between Mg# and Cr# and have significantly higher Mg#, and to a lesser extent lower Cr#, than the pyroxenites (Fig. 11b). Generally speaking, pyroxenites with increasing Cr# at increasing or nearly constant Mg# are related to melt-peridotite interaction (Garrido and Bodinier, 1999; Gysi et al., 2011; Lu et al., 2020; Tilhac et al., 2016), upon which the melt's Mg# is buffered by the peridotite (Kelemen, 1990). In contrast, the absence of such Mg#-Cr# correlation in San

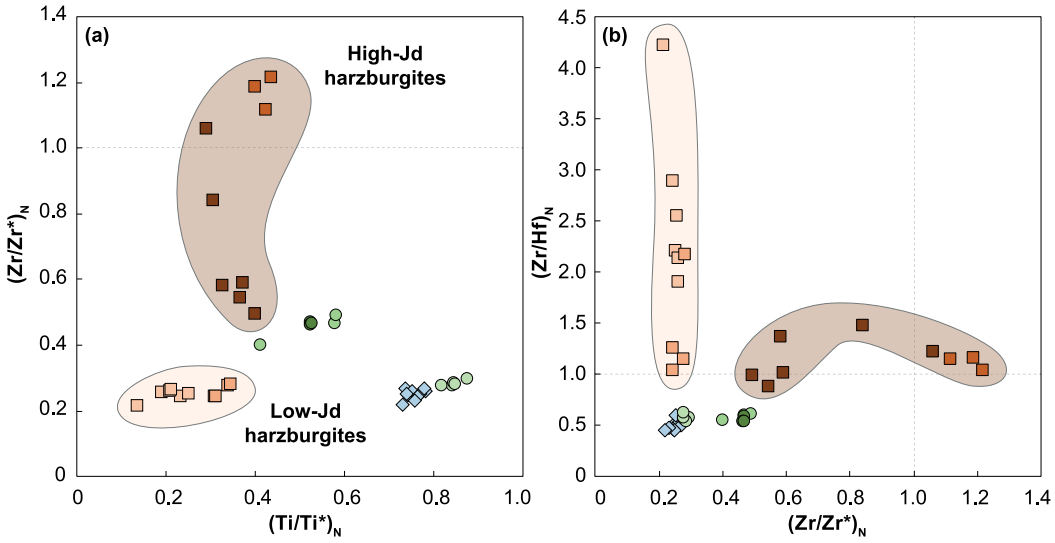

Fig. 9. Zr [Zr/Zr* with Zr* = (Sm × Nd)$^{0.5}$] *vs* Ti [Ti/Ti* with Ti* = (Dy × Gd)$^{0.5}$] anomalies (a) and Zr/Hf *vs* Zr anomalies in cpx. *N* denotes the normalization to chondrite composition (McDonough and Sun, 1995).

Carlos pyroxenites is incompatible with magmatic differentiation or melt-peridotite interaction. Instead, it reflects the contribution of spinel (characterized by positively correlated Mg# and Cr#; Fig. 11b) randomly incorporated into the pyroxenites (*i.e.* regardless of their Mg#) during metamorphic segregation. We specifically envisage that the remobilization of pyroxenes (±spinel) was locally promoted by *in-situ* partial melting and/or pressure-solution creep from the vicinity of the pyroxenite layers, which is supported by our observations across heterogeneous sample SH01. The latter exhibits a zoned, opx-rich pyroxenite layer rimmed by an olivine-rich area particularly depleted in spinel and pyroxenes (Fig. 5a). While such zoning could be interpreted as a reaction product between a Si-undersaturated melt and the host peridotite (*e.g.* Tilhac et al., 2016), it is inconsistent with the very limited chemical variations observed across the contact (Fig. 5b) and the strikingly homogeneous LREE depletion observed in pyroxenites and lherzolites (Fig. 8). Instead, these observations point towards a nearly isochemical remobilization of pyroxenes and spinel, consistent with the mineralogical variations across the pyroxenite layer (SH01-L). Slight variations observed in mineral chemistry are explained by differential sub-solidus re-equilibration subsequent to the formation of the pyroxene-rich layers. This is coherent with the subtle but significant differences in the internal zoning of the silicates, whose rims tend to have slightly higher Mg# in the pyroxenite, while the opposite situation is observed in the peridotitic part (Figs. 5b and 8a). We conclude that metamorphic segregation of pyroxenes accompanied melt-present deformation of San Carlos lherzolites. In this regard, we concur with Frey and Prinz (1978) who postulated the formation of "tectonic layers" based on the similarity between the lherzolitic and opx-rich pyroxenitic pyroxenes.

4.1.2. A continuum of magmatic and metamorphic processes

Purely mechanical segregation resulting from flow differentiation requires the presence of differential stress and mineral phases with different mechanical response to shear deformation. This process is responsible for the formation of lineation/foliation in mantle minerals but can hardly account alone for the formation of macroscopic layering. However, pressure-solution creep in the presence of deviatoric stress can induce local chemical gradients and differential crystal growth accommodating some extent of deformation. In turn, this process can result in metamorphic differentiation if accompanied by the development of a strong rheological contrast (*e.g.* olivine-rich *vs* pyroxene-rich bands), as documented in crustal rocks and envisaged by Dick and Sinton (1979) in partially molten mantle. Such mechanism has notably been invoked to account for the similarities between peridotitic and pyroxenitic pyroxenes in xenoliths from Hannuoba (Chen et al., 2001), or as discussed above, for the formation of pyroxene-rich horizons in San Carlos lherzolites.

We believe, however, that San Carlos pyroxenites (and pyroxenites in general) do form *via* distinct modes of formation or their combination (see Downes, 2007 for a review). For instance, convex-upward REE patterns with negative MREE-to-HREE slopes such as reported by Frey and Prinz (1978) relate to some extent of magmatic segregation following melt percolation (±melt-peridotite interaction). This feature, along with the positive correlation between Mg# and Cr# (as discussed above) or relatively high NiO concentrations in pyroxenitic olivine, are good indicators of (olivine-consuming) melt-peridotite interaction (*e.g.* Tilhac et al., 2016). Frey and Prinz (1978) had reached a similar conclusion in San Carlos to explain why the continuous compositional range between peridotitic and opx-rich pyroxenites is not observed towards their cpx-rich counterparts. Such cpx-rich pyroxenites could represent local magmatic segregations where sufficient melt connectivity had promoted some extent of disequilibrium between melt and peridotite.

Only limited constraints are available regarding the extent to which metamorphic (pressure solution-recrystallization) and magmatic segregation (crystallization from percolating/trapped melt) occurred in San Carlos mantle. From our detailed analysis of sample SH01, we believe that metamorphic segregation is volumetrically limited (probably on the order of a few centimeters to tens of centimeters at most). We are unaware of theoretical or experimental work aiming at characterizing the spatial limitation of this process. While it certainly cannot account for the isotopic disequilibrium frequently observed between pyroxenites and peridotites (Downes, 2007) or pyroxenite layer thicknesses exceeding several meters, pressure-solution creep may be a viable process to initiate the development of mineralogical heterogeneity during incipient partial melting, with important implications for the localization of deformation and fluid/melt circulation (*e.g.* Hidas et al., 2013). Furthermore, as the presence of small melt (or other fluid) fractions is a prerequisite to such process, we argue that metamorphic and magmatic segregation may operate as a continuum constrained by local

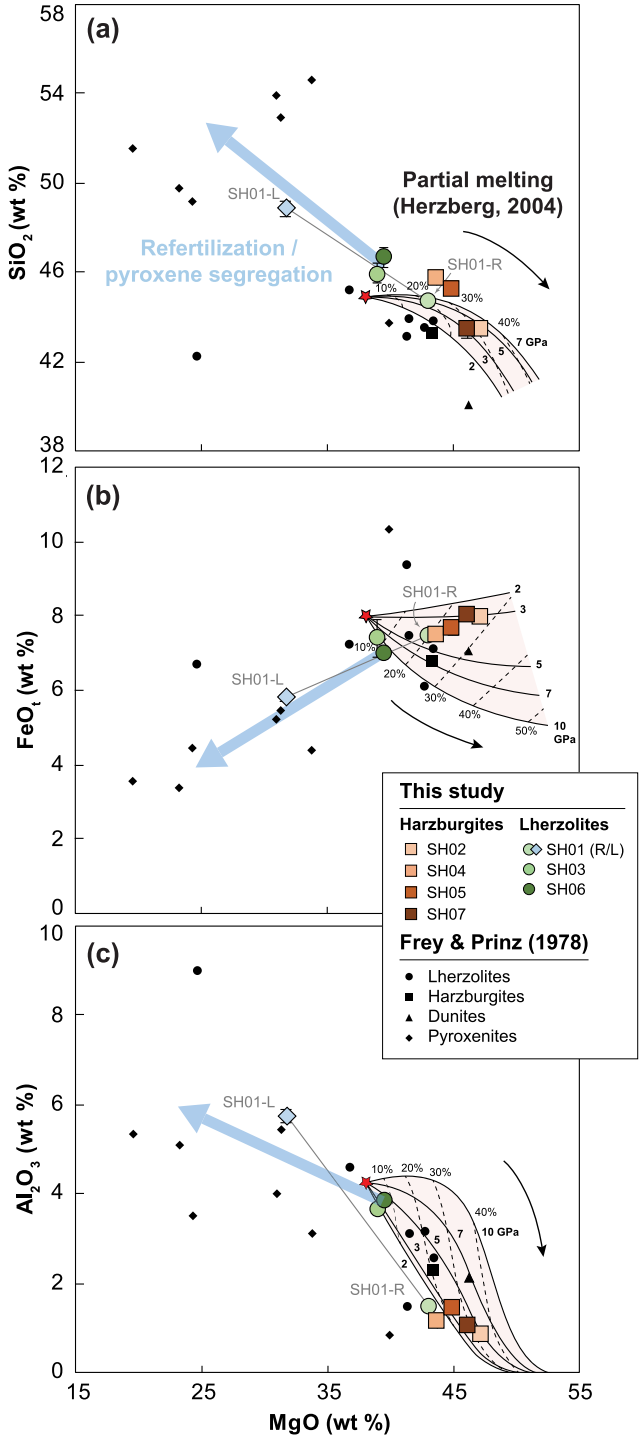

Fig. 10. Reconstructed bulk-rock (this study) and measured whole-rock compositions (Frey and Prinz, 1978) compared to fractional melting residues from a fertile source (KR-4003) as modelled by Herzberg (2004). For the latter, percentages and dashed lines indicate the melting degrees (*F*) while bold numbers and continuous lines indicate the initial melting pressure in GPa. The blue arrow depicts the potential effect of refertilization and/or pyroxene segregation.

stress conditions and melt connectivity, somewhat similar to the "mantle anatexis" discussed by Downes (2007). The existence of a porosity threshold in this continuous process could also contribute to coincident changes in rock structure from moderately fertile and homogeneous lherzolites to finely layered above ~4 wt% bulk Al_2O_3 (Bodinier and Godard, 2014).

4.2. Incipient flux melting and melt extraction in harzburgites

As discussed above, San Carlos lherzolites and harzburgites are consistent, to a first order, with variable degrees of partial melting. Accordingly, the bulk Na_2O decreases with increasing MgO content and is expectedly lower in the harzburgites (Electronic Appendix 2c). However, cpx in the high-Jd harzburgites have significantly higher Na_2O than their lherzolitic counterpart (Fig. 3d), which (along with other observations) cannot be accounted solely by simple melt-residue relationships.

4.2.1. Melt-present elemental redistribution and mineral chemistry

Several possibilities can account for high-Na cpx in relatively Na_2O-poor harzburgites. These high-Jd (3–7 mol%) cpx compared to other harzburgitic and lherzolitic cpx (0–5 mol%) could relate to the stabilization of the Jd component under higher pressures, leading to higher K^{Na}_{cpx} (Blundy et al., 1995). However, they do not exhibit higher proportions of Al^{IV} (*i.e.* Al in the tetrahedral site) as expected under higher pressures (*e.g.* Aoki and Kushiro, 1968) and actually have lower Ca-Tschermak (CaTs) proportions (< 4 mol%) than the lherzolitic cpx (CaTs = 4–6 mol%). Furthermore, higher K^{Na}_{cpx} would have also resulted in a lessened bulk-rock depletion in Na, which is not observed (Electronic Appendix 2c). Alternatively, high Na contents in cpx can be explained by re-equilibration under relatively low temperature, as the widening of the cpx-opx solvus leads to stronger distribution of Na in cpx (Hervig and Smith, 1980). This alternative is consistent with internal zoning observed in high-Jd cpx towards relatively Na_2O-rich rims (Figs. 6 & 7), but X-Ray mapping shows that this zoning is unrelated to the nature of the neighboring mineral (Fig. 7). All harzburgitic and lherzolitic cpx also exhibit comparable Ca contents (0.7–0.8 APFU) while higher contents are expected at lower temperatures. Furthermore, the high-Na_2O rims are also rich in Al_2O_3 (and Cr_2O_3), which cannot be solely accounted for by sub-solidus re-equilibration in a closed system. The consistency between the temperature estimates obtained from the two-pyroxene thermometer of Brey and Köhler (1990) and the REE-in-two-pyroxene of Liang et al. (2013) further supports this conclusion ($T_{BKN} = 1057 \pm 36$ °C; $T_{REE} = 1074 \pm 33$ °C). Extensive cooling would have indeed resulted in a shift of the Fe-Mg exchange thermometers towards lower values (Tilhac et al., 2017), which is not observed (Table 1). These relatively homogeneous temperature estimates indicate that these harzburgites did not follow a significantly different P-T path to the rest of San Carlos peridotites. The zoning of the high-Jd cpx is more likely to be the result of re-equilibration with a melt which is probably also responsible for the relatively high Na contents of these cpx compared to other harzburgitic and lherzolitic cpx (Fig. 3d). This interpretation is supported by EPMA profiles which show that high-Jd cpx cores are also affected by the diffusional re-equilibration induced by a chemical gradient initially present at the grain boundaries (Fig. 7).

The former presence of partial melt in San Carlos peridotites is attested by spongy textures along the cpx rims (Fig. 7d & e) which have been commonly related to the presence of melt (Kiseeva et al., 2017). Frey and Prinz (1978) noted the presence of glass as veins and along grain boundaries, characterized by high Na_2O (>5 wt%) and Al_2O_3 (>20 wt%) coherent with the chemical gradient inferred from the high-Jd cpx. Glass was also invoked by these authors to account for the discrepancy in Na_2O and Al_2O_3 between measured whole-rock and reconstructed bulk-rock compositions. A negative correlation between Na_2O and MgO is seen in both reconstructed bulk compositions and measured whole-rock compositions (Electronic Appendix 2c) and harzburgites remain poorer in Na_2O and Al_2O_3 than the lherzolites (*e.g.* Fig. 10c). A significant net addition of Na_2O (or Al_2O_3) to the harzburgite protoliths is thus excluded. The high-Jd cpx and their internal zoning most likely relate to elemental redistribution at the mineral/sample scale due to the presence of partial melt. We argue below that this process is the result of incipient hydrous flux melting as the

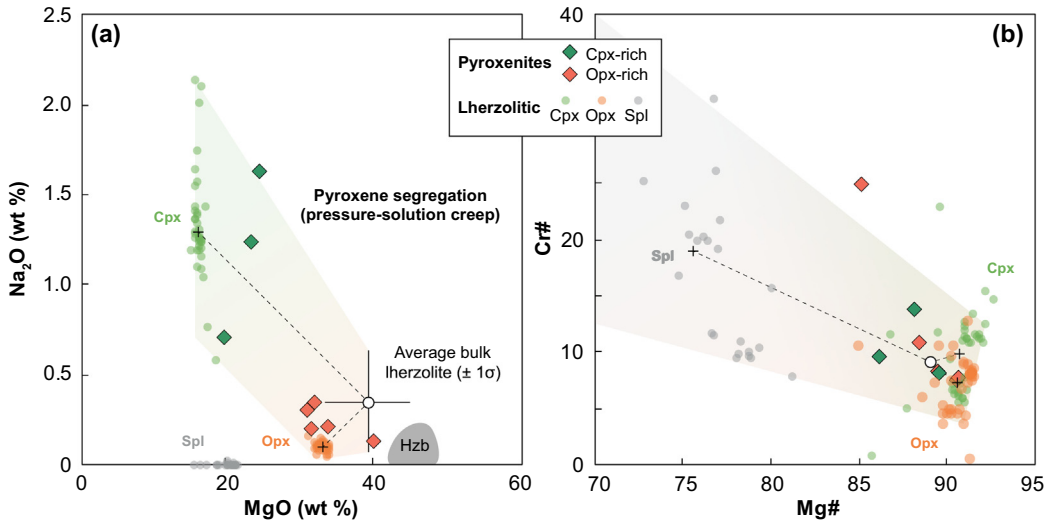

Fig. 11. Bulk pyroxenite compositions: Na_2O *vs* MgO (a) and Cr# *vs* Mg# (b), compared with simple mixing of the bulk lherzolite and average lherzolitic pyroxene compositions (black plus signs for cpx, opx and spinel) simulating the effect of pyroxene segregation in lherzolites. Note the negative correlation of Cr# and Mg# in pyroxenites unaccounted for by cpx-opx mixing, suggesting the contribution of spinel grains by mechanical mixing.

presence of water provides preferential conditions accounting for the modal and chemical variations observed.

During partial melting, the presence of water in the source region is known to depress the peridotite's melting point (Gaetani and Grove, 1998) so that any melting degree is reached at a lower temperature, and this thermal consequence is particularly strong for melting degrees <0.1% (Katz et al., 2003). Considering the temperature dependency of Na distribution in pyroxenes, we could anticipate that partial melting in hydrous conditions would result in relatively less Na_2O-depleted residual cpx (for a given melting degree). Harzburgitic cpx do exhibit higher (and more variable) distribution coefficients of Na than their lherzolitic counterpart although the latter host a larger proportion of the bulk Na_2O (66–92% against 35–59%) owing to higher cpx modes. However, it is experimentally known that cpx contribution to melting also decreases with increasing H_2O content and decreasing temperature (Gaetani and Grove, 1998), to the point that the exhaustion of opx may actually precede that of cpx (Liu et al., 2006). It is reasonable to assume that hydrous conditions during partial melting would also tend to impede bulk-rock Na depletion. If residual peridotites (and cpx) from hydrous melting exhibit relatively high Na (at a given melting degree) compared to dry residues, we can either envisage that the protolith of the high-Jd harzburgites was relatively Na-depleted and/or that melting degrees remained low. The former alternative is consistent with the cpx being originally more depleted in Na_2O as indicated by their chemical zoning, (Fig. 7). However, their relatively high HREE contents (Fig. 4) and the relatively low Cr# of spinel <55 (Fig. 8) exclude particularly high degrees of melting such as expected, for instance, in mantle-wedge environments (*e.g.* Le Roux et al., 2014). We argue that these observations reflect the persistence of cpx in the residual assemblage, probably promoted by hydrous conditions, and the fact that limited melt extraction occurred in the high-Jd harzburgites. In contrast, we interpret the low-Jd harzburgites as the residues of higher melting degrees and melt extraction rates. The absence of Na-rich rims in their cpx are consistent with their re-equilibration with higher-degree melts, which are expected from experiments to have lower Na_2O contents than to their near-solidus counterpart (Hirschmann et al., 1999). The low-Jd harzburgites are also characterized by higher Cr# in spinel and higher Mg# in cpx and opx indicative of slightly higher melting degrees. Yet, the low-Jd cpx do not exhibit the highest Cr_2O_3, which is instead observed in the high-Jd harzburgites, and so despite the fact that low- and high-Jd harzburgites have comparable bulk Cr_2O_3, confirming that little melt was extracted from the protolith of the high-Jd harzburgites. The high-Jd harzburgitic cpx are thus indicative of incipient flux melting upon which *in-situ* partial melts mostly contributed to elemental re-distribution through grain-boundary diffusion.

4.2.2. Trace-element partitioning during flux melting

From a trace-element mass-balance perspective, hydrous flux melting is a competition between elemental input and output from and to the aqueous fluid and extracted melt. Hydrous melting is characterized by different melting proportions compared to anhydrous melting, which has thermal, chemical and mineralogical implications for trace elements (*e.g.* Bizimis et al., 2000; Gaetani et al., 2003; Gaetani and Grove, 1998; Le Roux et al., 2014). Trace-element partitioning between minerals and melts is controlled by crystal chemistry as reflected, for instance, by the correlation between the cpx-melt partition coefficients and the concentrations of Ca^{2+} and Al^{3+} (Gaetani et al., 2003). As discussed above, hydrous melting may take place at lower temperatures (compared to dry melting), under which cpx is more calcic and should exhibit higher partition coefficients, notably for REE^{3+} incorporated in the M2 site. However, water tends to depolymerize the melt resulting in an overall decrease in most cpx-melt partition coefficients (Gaetani et al., 2003) but very little change in the overall trace-element patterns (McDade et al., 2003; Sun and Liang, 2012). In particular, the relative enrichment of large ion lithophile elements (LILE) over REE and HFSE cannot be accounted solely by hydrous melting of a peridotitic source and requires a net input from the fluxing agent. For instance, McDade et al. (2003) estimated that a high Sr/Nd and Zr/Hf slab component was required in the mantle beneath the South Sandwich Islands and St. Vincent, which is comparable to other estimates of slab components .

We here explore the implications of the trace-element fractionation observed in San Carlos between the different harzburgites with respect to the lherzolites in terms of the flux melting process. Specifically, the low-Jd cpx are homogeneous at the sample scale but exhibit a wide range of REE enrichment between samples, which contrasts the variable LREE enrichment observed at the sample and mineral scale in the high-Jd group. The latter is also characterized by a range of negative to positive Zr anomalies [$(Zr/Zr^*)_N = 0.5–1.2$] at nearly constant negative Ti anomalies [$(Ti/Ti^*)_N = 0.24–0.38$] and markedly positive Sr anomalies [$(Sr/Sr^*)_N = 0.9–3.1$]. Importantly, the trace-element compositions of cpx in equilibrium with the host basanite calculated with various sets of partition coefficients are markedly different, and especially less

LREE-enriched (Electronic Appendix 2d), to that of the high-Jd cpx (and particularly their rims). Mineral zoning is also observed regardless of the distance to the basanite contact and the possibility that this signature (and the cpx zoning) is related to a contamination by the host lava is excluded, which concurs with conclusions reached by Frey and Prinz (1978).

As demonstrated above, variations in the mineral chemistry of San Carlos harzburgites are well accounted for by various degrees of flux melting. This scenario is preferred to low-pressure melting, which would have similar modal implications to hydrous melting (*i.e.* lower consumption of cpx) but would still require the rather coincidental combination of partial melting and metasomatic overprint. We argue that variable influx of aqueous fluid led to variable degrees of melting and melt extraction. We have modelled this process using the mass-balance equations for open-system melting (OSM) of Ozawa (2001), and more specifically his 1D steady-state formulation (OSM-4). Hydrous melting was simulated using the melting equation of Gaetani and Grove (1998) and partition coefficients of McDade et al. (2003). Other modelling inputs and parameters are summarized in Table 2 and the three different setups best matching the lherzolites and of the high- and low-Jd harzburgites are shown in Fig. 12.

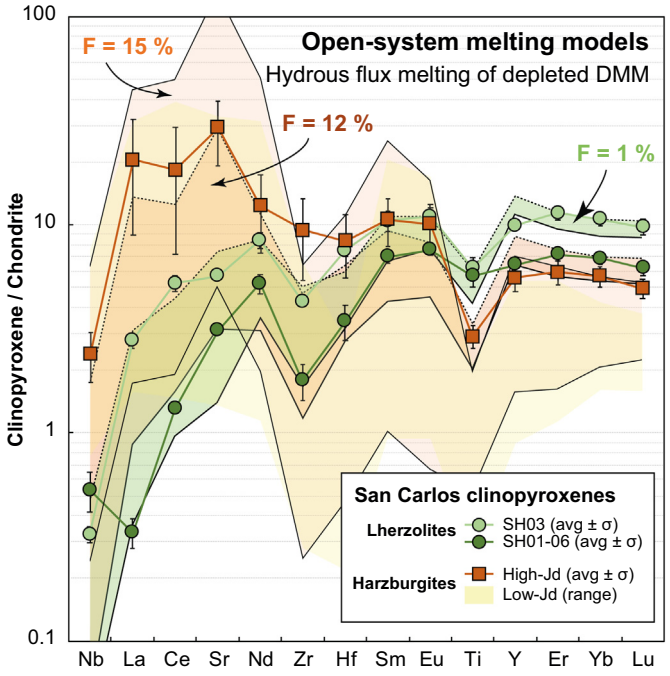

Fig. 12. Selected trace-element compositions of flux melting residues obtained from the 1D stead-state (OSM-4) open-system melting model of Ozawa (2001) and compared with the cpx compositions from San Carlos peridotites. Sample averages and standard deviations are shown for the lherzolites and high-Jd harzburgites while the whole range of compositions is shown for low-Jd harzburgites (yellow shading). For model 1 and 2 (F = 1% and 12%), continuous and dashed lines indicate the modelled compositions before and after trapped melt crystallization, respectively. For model 3 (F = 15%), results are shown for two influx rates. The model approach is detailed in the text; input compositions and fluxing parameters are summarized in Table 2.

Table 2
Trace-element modelling parameters.

1D steady-state hydrous flux melting (open-system melting OSM-4; Ozawa, 2001)		**Cpx**	**Opx**	**Ol**	**Spl**
		1.2 GPa (Gaetani and Grove, 1998)			
Source mode		0.08	0.27	0.63	0.02
Melting mode		0.62	0.51	−0.25	0.12

	Source composition	**Fluxing agent**	**Partition coefficients**			
ppm	5% batch DMM	Grove et al. (2002)	McDade et al. (2003)			
Nb	0.0001	38.3	0.008	0.0028	0.0002	0.20
La	0.0005	117	0.043	0.003	0.0001	0.0004
Ce	0.014	252	0.089	0.005	0.0002	0.001
Sr	0.63	7030	0.077	0.0044	0.00001	0.0001
Nd	0.11	133	0.211	0.009	0.0004	0.0006
Zr	0.63	856	0.103	0.027	0.004	0.005
Hf	0.042	25.4	0.206	0.062	0.006	0.01
Sm	0.084	24.9	0.363	0.021	0.0004	0.0005
Eu	0.041	6.57	0.449	0.031	0.001	0.0005
Ti	393	11,700	0.296	0.141	0.007	0.15
Y	2.34	74.0	0.561	0.101	0.005	0.01
Er	0.20	6.47	0.578	0.121	0.002	0.0004
Yb	0.22	6.00	0.543	0.164	0.004	0.0005
Lu	0.036	0.86	0.520	0.186	0.004	0.0005

OSM-4 parameters		*Model 1*	*Model 2*	*Model 3a*	*Model 3b*
f	Melting degree	1%	12%	15%	
α_c	Porosity threshold	0.01	0.02	0	
γ	Melt separation rate	0	0.1	1	
β	Influx rate	0	0.05	0.005	0.15
α_f	Trapped melt fraction	0.05	0.05	0.01	
τ	TMC separation rate	0.01	0.01	0.01	

The source composition of the OSM-4 model corresponds to the residual Depleted MORB Mantle (DMM; Workman and Hart, 2005) after 5% batch melting using a dry spinel lherzolite melting reaction and partition coefficients following Secchiari et al. (2020) and references therein. The composition of the fluxing agent corresponds to an average of slab-derived fluid-rich components. See text for further detail on the OSM-4 model setups and parameters.

Our results show that solely changing the extent of the process satisfactorily reproduces the whole range of harzburgitic cpx compositions (Fig. 12). Using a low influx rate ($\beta = 0.05$) and moderate melting degree (F = 12%) produces trace-element compositions comparable to that of cpx from high-Jd harzburgites, including the amplitude of the Nb, Ti and Sr anomalies and the slightly negative MREE-to-HREE slopes and relatively low bulk HREE contents. Interestingly, the best match is obtained if the melt separation rate is low ($\gamma = 0.1$) and a relatively high proportion of the melt remain trapped ($\alpha_f = 5\%$), which is consistent with the elemental redistribution in the presence of poorly extracted melt inferred from mineral chemistry and zoning of these high-Jd harzburgites (Figs. 3 & 6). In contrast, at higher melting degrees (F = 15%) and melt separation rate ($\gamma = 1$), the cpx compositions are very sensitive to fluxing and using $\gamma = 0.005$–0.15 reproduces the strong LREE-MREE enrichment and wide range of HREE depletion observed in the low-Jd harzburgites, especially if only small amount of melt is trapped ($\alpha_f = 1\%$). We note that the high Zr/Hf observed in our cpx, which are consistent with limited Zr depletion expected from hydrous melting (Le Roux et al., 2014), are not fully reproduced by the model results whose $(Zr/Hf)_N$ are restricted to <1. This discrepancy can be easily explained by our choice of using a single fluid composition while substantial variability exists in slab component estimates (*e.g.* 16–1007 ppm Zr; Bizimis et al., 2000; McDade et al., 2003), far exceeding the difference between our model and San Carlos cpx. Furthermore, subtle changes in partition coefficient (*e.g.* $Kd_{cpx\text{-}melt}$ of 0.2 instead of 0.1) are sufficient to change the residual $(Zr/Hf)_N$ from positive to negative. As such, this ratio is very sensitive to chromatographic re-equilibration or the presence of a Ti-rich accessory with overwhelming impact on HFSE fractionation, as suggested by the increase in $(Zr/Zr^*)_N$ at nearly constant $(Zr/Hf)_N$ and $(Ti/Ti^*)_N$ observed in the high-Jd cpx (Fig. 9), probably reflecting the transient re-equilibration of Zr and Hf.

4.2.3. Reactive channeling instability

Our OSM simulations are consistent with (1) the high-Jd harzburgites being the result of low fluid influx leading to incipient flux melting and producing poorly extracted low-volume melt and (2) the low-Jd harzburgites resulting from higher fluid influx and more efficient melt extraction. Interestingly, the model also shows that in the absence of fluxing, very limited melting degree (F = 1%) reproduces remarkably well the lherzolitic cpx compositions if trapped melt crystallization is taken into account (Fig. 12). We note that the ΣREE content, negative Zr-Hf and Ti anomalies and slightly negative MREE-to-HREE slope of the lherzolitic cpx are especially well reproduced if a hydrous melting equation and set of partition coefficients are used. It is thus likely that the lherzolites were affected during the flux melting process by low-volume, trapped melt crystallization (probably in the form of cpx), with little or no contribution from the fluxing agent. Considering that harzburgites and lherzolites have recorded similar P-T paths (as discussed above), this result suggests that the lherzolites probably remained below or near solidus because of being mostly preserved from hydration and that they best approximate San Carlos ambient mantle. Supporting this hypothesis, all the studied harzburgites exhibit high bulk K_2O/Na_2O (up to 0.16) compared to the lherzolites (<0.02), and a positive correlation between K_2O/Na_2O and MgO is observed in the whole-rock compositions reported by Frey and Prinz (1978).

Mineral chemistry and trace-element compositions observed between and within San Carlos lherzolites and harzburgites not only reflect various extents of flux melting, but they also suggest that the process was strongly localized, as discussed by Le Roux et al. (2014). It is indeed theoretically predicted that the presence of water (and volatile elements in general) during melt segregation promotes reactive channeling instability and the formation of preferential pathways of melt extraction (Keller and Katz, 2016). At 1 GPa and temperatures comparable to the equilibration temperatures estimated for San Carlos peridotites (~ 1070 °C; Table 1), very small amounts of water (< 0.3 wt%) are sufficient to increase F by >5%, while a dry lherzolite would mostly remain below solidus (Katz et al., 2003). Following this line of reasoning, we speculate that San Carlos harzburgites represent different portions of such channels or different stages of their development within a lherzolitic protolith. Pre-existing lithological heterogeneities resulting from earlier magmatic episodes probably also contributed to the development of such reactive channels which is known to be sensitive to the initial pyroxene content of the protolith.

4.3. Tectonic and geodynamic implications

4.3.1. Systematic enrichment of mantle harzburgites: single vs multi-stage scenarios

We have demonstrated above that San Carlos harzburgites and lherzolites can be regarded as cogenetic residues of various degrees of hydrous flux melting. Radiogenic isotope data reported for San Carlos by Galer and O'Nions (1989) are compatible with this assumption. They also specify that the harzburgites were recently isotopically re-equilibrated, as suggested by the restricted radiogenic Sr-, Nd- and Pb-isotope compositions. Most harzburgitic cpx have ε_{Nd} ranging between +6 and + 10, overlapping that of the host basanite (~ +9), while lherzolitic and pyroxenitic cpx have $\varepsilon_{Nd} = -2$ to +20 (see Fig. 13). The relative fertility of the lherzolites compared to DMM and PM estimates also suggests that San Carlos ambient mantle was probably once refertilized (Fig. 10), but we found only little petrological evidence of this process. In particular, we exclude that the lherzolites represent the refertilized products of San Carlos harzburgites, as it is inconsistent with the recent re-equilibration of the latter inferred from Nd isotopes (Galer and O'Nions, 1989). The mineralogical and geochemical features of San Carlos lherzolites are rather consistent with a low-degree partial melting process accompanying deformation and resulting in metamorphic segregations of opx-rich pyroxenites (± local cpx-rich magmatic segregation). Although the existence of several generations of pyroxenite cannot be excluded, several lines of evidence support the idea that pyroxenitic segregations occurred in lherzolite during the flux melting episode. Hydrous conditions are indeed compatible with magmatic segregation of cpx (Liu et al., 2006) and with the presence of opx inclusions in olivine in cpx-enriched lherzolites. The similarities between lherzolitic and pyroxenitic pyroxenes also specify that pyroxenite formation post-dates any potential refertilization. In fact, if pyroxenites had been present prior to the fluxing episode, they would have experienced much higher melting degrees which are not observed. In this regard, our conclusion is consistent with field observations from ophiolitic lherzolites where replacive harzburgites (and dunites) bodies (Kelemen et al., 1992; Le Roux et al., 2014; Secchiari et al., 2020) are locally associated with cpx segregations (*e.g.* Quick, 1981).

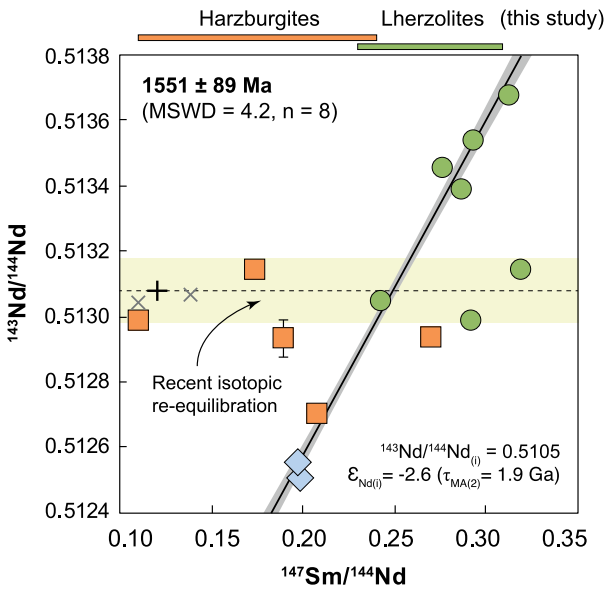

Fig. 13. Sm-Nd isochron plot modified from Galer and O'Nions (1989). An isochron age is obtained for the pyroxenites and lherzolites if two samples are excluded. In contrast, most harzburgites have a homogeneous $^{143}Nd/^{144}Nd$ around 0.5131 over a wide range of $^{147}Sm/^{144}Nd$, suggesting a recent isotopic reset. The black plus sign indicates the compositions of the host basanites; the grey crosses are data for the nearby Soda Springs vent from the same study. Data from Galer and O'Nions (1989). The orange and green bars show the range of Sm/Nd from this study.

The lithological and chemical heterogeneity of San Carlos mantle reflects a single-stage fluxing scenario consisting in the development of reactive harzburgitic channels and localized magmatic/metamorphic segregations accompanying deformation. While other interpretations are certainly possible (*e.g.* Secchiari et al., 2020), we argue that other paradoxical association of LREE-depleted lherzolites and LREE-enriched harzburgites may also reflect complex spatio-temporal variations during flux melting (in the presence of pre-existing heterogeneities and/or volatiles), rather than discrete melting and metasomatic episodes (see also Bodinier et al., 2004).

4.3.2. Reactivation of ancient lithosphere and the sources of the Jemez Lineament

With few exceptions, lherzolites and pyroxenites exhibit a fairly good correlation between $^{143}Nd/^{144}Nd$ and $^{147}Sm/^{144}Nd$, which would correspond to an isochron age of 1551 ± 89 Ma (Fig. 13). While mixing between a low-Sm/Nd pyroxenitic component and high-Sm/Nd depleted peridotite cannot be entirely ruled out, it is inconsistent with the lack of correlation between the $^{143}Nd/^{144}Nd$ and 1/Nd. There are two ways to interpret this potential 1.55-Ga isochron, which was not reported by Galer and O'Nions (1989) due to the overall scattering of the data: it could either record the flux melting episode or an earlier

(refertilization) episode. The second alternative is preferred as it is supported by the relatively small range of $^{147}Sm/^{144}Nd$ consistent with the homogeneous LREE depletion observed in the lherzolites (Fig. 13). It is also consistent with the relative fertility and tectono-thermal age of the lithosphere in this part of the North American continent, and more specifically the Yavapai-Mazatzal terranes (Griffin et al., 2004). A refertilization process was also proposed from Lu-Hf compositions of xenoliths from the Rio Grande Rift and Colorado Plateau (Byerly and Lassiter, 2015) and we speculate that the pre-refertilization protolith could be dated *ca* 1.9 Ga by the model age obtained for the initial $^{143}Nd/^{144}Nd$ (0.5106) of the above-mentioned isochron. In spite of their relatively poor statistical robustness, these ages are strikingly well documented in detrital zircons from north-western USA (Laskowski et al., 2013), U-Pb ages and Hf-isotope data on zircons from eclogite and garnetite xenoliths (Smith and Griffin, 2005) and Sm-Nd ages and *Re*-depletion ages from Colorado Plateau mantle xenoliths (Marshall et al., 2017).

In contrast, the recent isotopic re-equilibration of the harzburgites over a relatively wide range of $^{147}Sm/^{144}Nd$ (Fig. 13) is ascribed to variable LREE enrichment during the flux melting episode. This scenario is preferred to the alternative interpretation upon which the 1.55-Ga isochron dates the flux melting episode, incompatible with the preservation of compositional gradient (Fig. 7) which would have been homogenized in a few million years considering the diffusivities of Fe-Mg ($D \sim 10^{-19}$ m^2/s at 1100 °C) and Al ($D \sim 10^{-21}$ m^2/s; Lierenfeld et al., 2019). The Nd-isotope compositions of the harzburgites are within error of that of the host basanites and other local volcanics dated at 0.58 ± 0.21 Ma (Bernatowicz, 1981) which is consistent with the near-zero age inferred from the spread in $^{147}Sm/^{144}Nd$ over a relatively narrow range of $^{143}Nd/^{144}Nd$. It is tempting to relate the flux melting episode to the basanite petrogenesis, but direct cogenetic relationships between San Carlos Group-I xenoliths and their host lava are unlikely. The trace-element compositions of the latter, characterized by homogeneously enriched REE patterns and the absence of HFSE and Sr anomalies, are clearly incompatible with melt-residua relationships involving San Carlos peridotites, in good agreement with the conclusions reached by Frey and Prinz (1978). Nonetheless, their isotopic similarities are probably not coincidental and the processes identified in this study may be relevant to the petrogenesis of San Carlos basanites.

Flux melting, such as inferred from the mineral chemistry and trace-element compositions of San Carlos peridotites, is commonly invoked in subduction settings (see Grove et al., 2012 for a review) and relative HFSE depletion and LILE enrichment are often regarded as a characteristic fingerprint of subduction-related volcanic rocks (*e.g.* Garrido et al., 2005, and references therein). However, HFSE-depleted peridotites are reported in other tectonic settings (Salters and Shimizu, 1988) and hydrothermal interaction can, for instance, result in hydrous melting in mid-ocean ridge environments (*e.g.* Rospabé et al., 2018). Fluid sources responsible for the HFSE-depleted, subduction-like signature of San Carlos peridotites are beyond the scope of this paper. Nonetheless, we note that San Carlos volcanic field constitutes the southwestern termination of the Jemez Lineament, an 800-km long chain of Tertiary-Quaternary volcanoes (Spence and Gross, 1990). This ~100-km-wide zone characterized by active uplift, low seismic velocity in the mantle and repeated tectonic reactivation, is the most active volcanic feature in the southwestern USA (Magnani et al., 2004 and references therein). HFSE-depleted mantle xenoliths like San Carlos have been reported in other localities along the Jemez Lineament such as Cerro Chato, contrasting with xenoliths such as those from Elephant Butte that are sampled off this structure (Byerly and Lassiter, 2014). The Jemez Lineament has been interpreted as the crustal expression of the collision of Mazatzal island arcs with Yavapai proto-North American continent at *ca* 1.68–1.65 Ga (Magnani et al., 2004). Subduction tectonics have been active in the area during the Proterozoic, but no such environment is documented to account for the recent evolution of San Carlos peridotites. It is thus likely that flux melting did not occur in an active subduction zone but instead during a later tectonic reactivation of the lithosphere where the existence of near-solidus conditions promoted by the presence of hydrous fluids is consistent with our temperature estimates. In fact, the mantle source of the Jemez Lineament has previously been proposed to be located within the lithosphere to explain why it seem to be entrained by the motion of the North American plate (Spence and Gross, 1990). Partial melting of the lithospheric mantle was probably volumetrically limited but the involvement of some extent of flux melting in the petrogenesis of San Carlos basanites is also consistent with their high alkaline contents (Hadnott et al., 2017) and the high volatile concentrations inferred from the explosiveness of their eruption (Wohletz, 1978). In this regard, the similar Nd-isotope compositions (but distinct trace-element signature) of San Carlos harzburgites and their host basanites either reflect melt-peridotite interaction and/or the involvement of the same fluid sources during the tectonic reactivation of the Proterozoic subduction zone.

5. Conclusions

We have reported new petrographic observations and modal, major- and trace-element compositions from San Carlos peridotites. Along with the results of open-system melting simulations, these data support a single-stage evolution upon which the lithological and chemical heterogeneity of San Carlos mantle is mostly the result of various extent of flux melting. The following conclusions were reached:

1. The San Carlos peridotites originated from a lherzolitic protolith whose fertility is likely to be the result of a refertilization episode potentially recorded by a Sm-Nd isochron at 1.55 Ga, consistent with other geochronological data for the western USA.
2. Hydrous flux melting occurred in the lithosphere during the tectonic reactivation of a Proterozoic subduction zone coeval with volcanic activity along the Jemez Lineament.
3. Pressure-solution creep during melt-present deformation led to the formation of opx-rich pyroxenites in the lherzolites while cpx-rich magmatic pyroxenites formed locally.
4. Metamorphic and magmatic segregation of pyroxenes may operate as a continuum constrained by local stress conditions and melt connectivity; the existence of a porosity threshold in this process probably contributes to systematic changes in rock structure.
5. The harzburgitic cpx have either lower or higher Jd components than their lherzolitic counterparts, which is interpreted as the result of local elemental redistribution due to the presence of a low-degree hydrous melt along grain boundaries.
6. Open-system melting simulations of trace-element fractionation show that the high-Jd harzburgites result from low fluid influx leading to incipient melting and poor melt extraction, while the low-Jd harzburgites result from higher fluid influx.
7. The paradoxical occurrence of LREE-depleted lherzolites and LREE-enriched harzburgites may often reflect spatio-temporal variations in the development of lithospheric melt pathways promoted by reactive channeling instability during flux melting in the presence of existing heterogeneities and/or volatiles.

Declaration of Competing Interest

The authors declare that they have no known competing financial interests or personal relationships that could have appeared to influence the work reported in this paper.

Acknowledgements

We are grateful to K. Itano for fruitful discussion of the ideas developed in this paper and K. Ozawa for support on the use of his open-system melting model. The manuscript benefited from constructive comments provided by Q. Xiong and three anonymous reviewers as

well as from the editor X.-H. Li. This work was funded by a Japan Society for the Promotion of Science (JSPS) fellowship.

Appendix A. Supplementary data

Supplementary data to this article can be found online at https://doi.org/10.1016/j.lithos.2021.106195.

References

Aoki, K.i., Kushiro, I., 1968. Some clinopyroxenes from ultramafic inclusions in Dreiser Weiher, Eifel. Contrib. Mineral. Petrol. 18, 326–337.

Arai, S., 1994. Characterization of spinel peridotites by olivine-spinel compositional relationships: Review and interpretation. Chem. Geol. 113, 191–204.

Bernatowicz, T.J., 1981. Noble gases in ultramafic xenoliths from San Carlos, Arizona. Contrib. Mineral. Petrol. 76, 84–91.

Bizimis, M., Salters, V.J.M., Bonatti, E., 2000. Trace and REE content of clinopyroxenes from supra-subduction zone peridotites. Implications for melting and enrichment processes in island arcs. Chem. Geol. 165, 67–85.

Blundy, J.D., Falloon, T.J., Wood, B.J., Dalton, J.A., 1995. Sodium partitioning between clinopyroxene and silicate melts. J. Geophys. Res. Solid Earth 100, 15501–15515.

Bodinier, J.-L., Godard, M., 2014. Orogenic, ophiolitic, and abyssal peridotites. In: Turekian, K.K. (Ed.), Treatise on Geochemistry, Second edition Elsevier, Oxford, pp. 103–167.

Bodinier, J.-L., Menzies, M.A., Shimizu, N., Frey, F.A., McPherson, E., 2004. Silicate, hydrous and carbonate metasomatism at Lherz, France: contemporaneous derivatives of silicate melt–harzburgite reaction. J. Petrol. 45, 299–320.

Borghini, G., Rampone, E., Zanetti, A., Class, C., Fumagalli, P., Godard, M., 2020. Ligurian pyroxenite-peridotite sequences (Italy) and the role of melt-rock reaction in creating enriched-MORB mantle sources. Chem. Geol. 532, 119252.

Brey, G.P., Köhler, T., 1990. Geothermobarometry in four-phase lherzolites II. New thermobarometers, and practical assessment of existing thermobarometers. J. Petrol. 31, 1353–1378.

Byerly, B.L., Lassiter, J.C., 2014. Isotopically ultradepleted domains in the convecting upper mantle: Implications for MORB petrogenesis. Geology. 42 (3), 203–206.

Byerly, B.L., Lassiter, J.C., 2015. Trace element partitioning and Lu–Hf isotope systematics in spinel peridotites from the Rio Grande Rift and Colorado Plateau: Towards improved age assessment of clinopyroxene Lu/Hf–176Hf/177Hf in SCLM peridotite. Chem. Geol. 413, 146–158.

Chen, S., O'Reilly, S.Y., Zhou, X., Griffin, W.L., Zhang, G., Sun, M., Feng, J., Zhang, M., 2001. Thermal and petrological structure of the lithosphere beneath Hannuoba, Sino-Korean Craton, China: evidence from xenoliths. Lithos 56, 267–301.

Chetouani, K., Bodinier, J.-L., Garrido, C.J., Marchesi, C., Amri, I., Targuisti, K., 2016. Spatial variability of pyroxenite layers in the Beni Bousera orogenic peridotite (Morocco) and implications for their origin. Comptes Rendus Géoscience 348, 619–629.

Dick, H.J.B., Sinton, J.M., 1979. Compositional layering in alpine peridotites: evidence for pressure solution creep in the mantle. J. Geol. 87, 403–416.

Downes, H., 2001. Formation and Modification of the Shallow Sub-continental Lithospheric Mantle: a Review of Geochemical evidence from Ultramafic Xenolith Suites and Tectonically Emplaced Ultramafic Massifs of Western and Central Europe. J. Petrol. 42, 233–250.

Downes, H., 2007. Origin and significance of spinel and garnet pyroxenites in the shallow lithospheric mantle: Ultramafic massifs in orogenic belts in Western Europe and NW Africa. Lithos 99, 1–24.

Dygert, N., Liang, Y., Kelemen, P.B., 2016. Formation of Plagioclase Lherzolite and Associated Dunite–Harzburgite–Lherzolite Sequences by Multiple Episodes of Melt Percolation and Melt–Rock Reaction: An Example from the Trinity Ophiolite, California, USA. J. Petrol. 57 (4), 815–838.

Frey, F.A., Prinz, M., 1978. Ultramafic inclusions from San Carlos, Arizona: Petrologic and geochemical data bearing on their petrogenesis. Earth Planet. Sci. Lett. 38, 129–176.

Gaetani, G.A., Grove, T.L., 1998. The influence of water on melting of mantle peridotite. Contrib. Mineral. Petrol. 131, 323–346.

Gaetani, G.A., Kent, A.J.R., Grove, T.L., Hutcheon, I.D., Stolper, E.M., 2003. Mineral/melt partitioning of trace elements during hydrous peridotite partial melting. Contrib. Mineral. Petrol. 145, 391–405.

Galer, S.J.G., O'Nions, R.K., 1989. Chemical and isotopic studies of ultramafic inclusions from the san carlos volcanic field, arizona: a bearing on their petrogenesis. J. Petrol. 30, 1033–1064.

Garapić, G., Faul, U.H., Brisson, E., 2013. High-resolution imaging of the melt distribution in partially molten upper mantle rocks: evidence for wetted two-grain boundaries. Geochem. Geophys. Geosyst. 14, 556–566.

Garrido, C.J., Bodinier, J.-L., 1999. Diversity of mafic rocks in the Ronda peridotite: evidence for pervasive melt–rock reaction during heating of subcontinental lithosphere by upwelling asthenosphere. J. Petrol. 40, 729–754.

Garrido, C.J., Bodinier, J.-L., Alard, O., 2000. Incompatible trace element partitioning and residence in anhydrous spinel peridotites and websterites from the Ronda orogenic peridotite. Earth Planet. Sci. Lett. 181, 341–358.

Garrido, C.J., López Sánchez-Vizcaíno, V., Gómez-Pugnaire, M.T., Trommsdorff, V., Alard, O., Bodinier, J.-L., Godard, M., 2005. Enrichment of HFSE in chlorite-harzburgite produced by high-pressure dehydration of antigorite-serpentinite: Implications for subduction magmatism. Geochem. Geophys. Geosyst. 6.

Goldschmidt, V.M., 1922. On the metasomatic processes in silicate rocks. Econ. Geol. 17, 105–123.

Griffin, W.L., O'Reilly, S.Y., Abe, N., Aulbach, S., Davies, R.M., Pearson, N.J., Doyle, B.J., Kivi, K., 2003. The origin and evolution of Archean lithospheric mantle. Precambrian Res. 127, 19–41.

Griffin, W., O'Reilly, S.Y., Doyle, B., Pearson, N., Coopersmith, H., Kivi, K., Malkovets, V., Pokhilenko, N., 2004. Lithosphere mapping beneath the north American plate. Lithos 77, 873–922.

Grove, T.L., Parman, S.W., Bowring, S.A., Price, R.C., Baker, M.B., 2002. The role of an H2O-rich fluid component in the generation of primitive basaltic andesites and andesites from the Mt. Shasta region, N California. Contrib. Mineral. Petrol. 142, 375–396.

Grove, T.L., Till, C.B., Krawczynski, M.J., 2012. The Role of H2O in Subduction Zone Magmatism. Annu. Rev. Earth Planet. Sci. 40, 413–439.

Gruau, G., Bernard-Griffiths, J., Lécuyer, C., 1998. The origin of U-shaped rare earth patterns in ophiolite peridotites: assessing the role of secondary alteration and melt/rock reaction. Geochim. Cosmochim. Acta 62, 3545–3560.

Gysi, A.P., Jagoutz, O., Schmidt, M.W., Targuisti, K., 2011. Petrogenesis of Pyroxenites and Melt Infiltrations in the Ultramafic complex of Beni Bousera, Northern Morocco. J. Petrol. 52, 1679–1735.

Hadnott, B.A., Ehlmann, B.L., Jolliff, B.L., 2017. Mineralogy and chemistry of San Carlos high-alkali basalts: analyses of alteration with application for Mars exploration. Am. Mineral. 102, 284–301.

Harlov, D.E., Austrheim, H., 2013. Metasomatism and the Chemical Transformation of Rock: Rock-Mineral-Fluid Interaction in Terrestrial and Extraterrestrial Environments, Metasomatism and the Chemical Transformation of Rock. Springer, pp. 1–16.

Hellebrand, E., Snow, J.E., Dick, H.J., Hofmann, A.W., 2001. Coupled major and trace elements as indicators of the extent of melting in mid-ocean-ridge peridotites. Nature 410, 677–681.

Hervig, R.L., Smith, J.V., 1980. Sodium thermometer for pyroxenes in garnet and spinel lherzolites. J. Geol. 88, 337–342.

Herzberg, C., 2004. Geodynamic information in peridotite petrology. J. Petrol. 45, 2507–2530.

Hidas, K., Garrido, C.J., Tommasi, A., Padrón-Navarta, J.A., Thielmann, M., Konc, Z., Frets, E., Marchesi, C., 2013. Strain Localization in Pyroxenite by Reaction-Enhanced Softening in the Shallow Subcontinental Lithospheric Mantle. J. Petrol. 54 (10), 1997–2031.

Hirschmann, M.M., Ghiorso, M.S., Stolper, M., 1999. Calculation of peridotite partial melting from thermodynamic models of minerals and melts. II. Isobaric variations in melts near the solidus and owing to variable source composition. J. Petrol. 40, 297–313.

Katz, R.F., Weatherley, S.M., 2012. Consequences of mantle heterogeneity for melt extraction at mid-ocean ridges. Earth Planet. Sci. Lett. 335-336, 226–237.

Katz, R.F., Spiegelman, M., Langmuir, C.H., 2003. A new parameterization of hydrous mantle melting. Geochem. Geophys. Geosyst. 4 (n/a-n/a).

Kelemen, P.B., 1990. Reaction between ultramafic rock and fractionating basaltic Magma I. phase relations, the origin of Calc-alkaline Magma series, and the Formation of Discordant Dunite. J. Petrol. 31, 51–98.

Kelemen, P.B., Dick, H.J., Quick, J.E., 1992. Formation of harzburgite by pervasive melt/rock reaction in the upper mantle. Nature 358, 635–641.

Keller, T., Katz, R.F., 2016. The role of volatiles in reactive melt transport in the asthenosphere. J. Petrol. 57, 1073–1108.

Kiseeva, E.S., Kamenetsky, V.S., Yaxley, G.M., Shee, S.R., 2017. Mantle melting versus mantle metasomatism – "the chicken or the egg" dilemma. Chem. Geol. 455, 120–130.

Lambart, S., Laporte, D., Schiano, P., 2013. Markers of the pyroxenite contribution in the major-element compositions of oceanic basalts: Review of the experimental constraints. Lithos 160–161, 14–36.

Laskowski, A.K., DeCelles, P.G., Gehrels, G.E., 2013. Detrital zircon geochronology of Cordilleran retroarc foreland basin strata, western North America. Tectonics 32, 1027–1048.

Le Roux, V., Bodinier, J.-L., Tommasi, A., Alard, O., Dautria, J.-M., Vauchez, A., Riches, A., 2007. The Lherz spinel lherzolite: refertilized rather than pristine mantle. Earth Planet. Sci. Lett. 259, 599–612.

Le Roux, V., Dick, H.J.B., Shimizu, N., 2014. Tracking flux melting and melt percolation in supra-subduction peridotites (Josephine ophiolite, USA). Contrib. Mineral. Petrol. 168, 1–22.

Liang, Y., Sun, C., Yao, L., 2013. A REE-in-two-pyroxene thermometer for mafic and ultramafic rocks. Geochim. Cosmochim. Acta 102, 246–260.

Lierenfeld, M.B., Zhong, X., Reusser, E., Kunze, K., Putlitz, B., Ulmer, P., 2019. Species diffusion in clinopyroxene solid solution in the diopside-anorthite system. Contrib. Mineral. Petrol. 174, 46.

Liu, X., O'Neill, H.S.C., Berry, A.J., 2006. The effects of small amounts of H2O, CO2 and Na2O on the partial melting of spinel lherzolite in the system CaO–MgO–Al2O3–SiO2 ± H2O ± CO2 ± Na2O at 1·1GPa. J. Petrol. 47, 409–434.

Lu, J., Griffin, W.L., Tilhac, R., Xiong, Q., Zheng, J., O'Reilly, S.Y., 2018. Tracking deep lithospheric events with garnet-websterite xenoliths from Southeastern Australia. J. Petrol. 59, 901–930.

Lu, J., Tilhac, R., Griffin, W.L., Zheng, J., Xiong, Q., Oliveira, B., O'Reilly, S.Y., 2020. Lithospheric memory of subduction in mantle pyroxenite xenoliths from rift-related basalts. Earth Planet. Sci. Lett. 544, 116365.

Magnani, M., Miller, K., Levander, A., Karlstrom, K., 2004. The Yavapai-Mazatzal boundary: a long-lived tectonic element in the lithosphere of southwestern North America. Geol. Soc. Am. Bull. 116, 1137–1142.

Marshall, E.W., Lassiter, J.C., Barnes, J.D., Luguet, A., Lissner, M., 2017. Mantle melt production during the 1.4 Ga Laurentian magmatic event: Isotopic constraints from Colorado Plateau mantle xenoliths. Geology. 45 (6), 519–522.

McDade, P., Blundy, J.D., Wood, B.J., 2003. Trace element partitioning between mantle wedge peridotite and hydrous MgO-rich melt. Am. Mineral. 88, 1825–1831.

McDonough, W.F., Sun, S.s., 1995. The composition of the Earth. Chem. Geol. 120, 223–253.

Oliveira, B., Afonso, J.C., Tilhac, R., 2020. A disequilibrium reactive transport model for mantle magmatism. J. Petrol. 61 (9), egaa067.
Ozawa, K., 2001. Mass balance equations for open magmatic systems: Trace element behavior and its application to open system melting in the upper mantle. J. Geophys. Res. Solid Earth 106, 13407–13434.
Prinzhofer, A., Allègre, C.J., 1985. Residual peridotites and the mechanisms of partial melting. Earth Planet. Sci. Lett. 74, 251–265.
Quick, J.E., 1981. Petrology and petrogenesis of the Trinity peridotite, an upper mantle diapir in the eastern Klamath Mountains, northern California. J. Geophys. Res. Solid Earth 86, 11837–11863 1978–2012.
Rospabé, M., Benoit, M., Ceuleneer, G., Hodel, F., Kaczmarek, M.-A., 2018. Extreme geochemical variability through the dunitic transition zone of the Oman ophiolite: Implications for melt/fluid-rock reactions at Moho level beneath oceanic spreading centers. Geochim. Cosmochim. Acta 234, 1–23.
Salters, V.J.M., Shimizu, N., 1988. World-wide occurrence of HFSE-depleted mantle. Geochim. Cosmochim. Acta 52, 2177–2182.
Sanfilippo, A., Salters, V., Tribuzio, R., Zanetti, A., 2019. Role of ancient, ultra-depleted mantle in Mid-Ocean-Ridge magmatism. Earth Planet. Sci. Lett. 511, 89–98.
Secchiari, A., Montanini, A., Bosch, D., Macera, P., Cluzel, D., 2020. Sr, Nd, Pb and trace element systematics of the New Caledonia harzburgites: Tracking source depletion and contamination processes in a SSZ setting. Geosci. Front. 11, 37–55.
Smith, D., Griffin, W.L., 2005. Garnetite Xenoliths and Mantle–Water Interactions Below the Colorado Plateau, Southwestern United States. J. Petrol. 46, 1901–1924.
Song, Y., Frey, F.A., 1989. Geochemistry of peridotite xenoliths in basalt from Hannuoba, Eastern China: Implications for subcontinental mantle heterogeneity. Geochim. Cosmochim. Acta 53, 97–113.
Spence, W., Gross, R.S., 1990. A tomographic glimpse of the upper mantle source of magmas of the Jemez lineament, New Mexico. J. Geophys. Res. Solid Earth 95, 10829–10849.
Sun, C., Liang, Y., 2012. Distribution of REE between clinopyroxene and basaltic melt along a mantle adiabat: effects of major element composition, water, and temperature. Contrib. Mineral. Petrol. 163, 807–823.
Tilhac, R., Ceuleneer, G., Griffin, W.L., O'Reilly, S.Y., Pearson, N.J., Benoit, M., Henry, H., Girardeau, J., Grégoire, M., 2016. Primitive arc magmatism and delamination: petrology and geochemistry of pyroxenites from the Cabo Ortegal complex, Spain. J. Petrol. 57, 1921–1954.
Tilhac, R., Grégoire, M., O'Reilly, S.Y., Griffin, W.L., Henry, H., Ceuleneer, G., 2017. Sources and timing of pyroxenite formation in the sub-arc mantle: Case study of the Cabo Ortegal complex, Spain. Earth Planet. Sci. Lett. 474, 490–502.
Tilhac, R., Oliveira, B., Griffin, W.L., O'Reilly, S.Y., Schaefer, B.F., Alard, O., Ceuleneer, G., Afonso, J.C., Grégoire, M., 2020. Reworking of old continental lithosphere: Unradiogenic Os and decoupled Hf Nd isotopes in sub-arc mantle pyroxenites. Lithos 354-355, 105346.
Toramaru, A., Fujii, N., 1986. Connectivity of melt phase in a partially molten peridotite. J. Geophys. Res. Solid Earth 91, 9239–9252.
Toramaru, A., Takazawa, E., Morishita, T., Matsukage, K., 2001. Model of layering formation in a mantle peridotite (Horoman, Hokkaido, Japan). Earth Planet. Sci. Lett. 185, 299–313.
Van Orman, J.A., Grove, T.L., Shimizu, N., 2001. Rare earth element diffusion in diopside: influence of temperature, pressure, and ionic radius, and an elastic model for diffusion in silicates. Contrib. Mineral. Petrol. 141, 687–703.
Vasseur, G., Vernières, J., Bodiner, J.-L., 1991. Modelling of trace element transfer between mantle melt and heterogranular peridotite matrix. J. Petrol. Special Lherzolites Issue 41–54.
Vernières, J., Godard, M., Bodinier, J.L., 1997. A plate model for the simulation of trace element fractionation during partial melting and magma transport in the Earth's upper mantle. J. Geophys. Res. Solid Earth 102, 24771–24784 1978–2012.
Wilshire, H.G., Jackson, E.D., 1975. Problems in determining mantle geotherms from pyroxene compositions of ultramafic rocks. J. Geol. 83, 313–329.
Wohletz, K., 1978. The eruptive mechanism of the Peridot Mesa vent, San Carlos, Arizona. Geological Society of America. Cordilleran Section Special Paper, pp. 167–176.
Workman, R.K., Hart, S.R., 2005. Major and trace element composition of the depleted MORB mantle (DMM). Earth Planet. Sci. Lett. 231, 53–72.